Available online at www.sciencedirect.com
SCIENCE DIRECT
Journal of Asian Earth Sciences 27 (2006) 265–285
Journal of Asian Earth Sciences
www.elsevier.com/locate/jaes

The Eastern Himalayan syntaxis: major tectonic domains, ophiolitic mélanges and geologic evolution

Geng Quanru[a,b,*], Pan Guitang[b], Lailin Zheng[b], Zhiliang Chen[b], Richard D. Fisher[c], Zhiming Sun[b], Chunsheng Ou[d], Han Dong[d], Xiaowei Wang[d], Sheng Li[b], Xiongying Lou[b], Heng Fu[b]

[a]*Faculty of Earth Sciences, China University of Geosciences, Wuhan 430074 Hubei, People's Republic of China*
[b]*Chengdu Institute of Geology and Mineral Resources, 82/3 No.1 Ring Road (N), Chengdu 610082, People's Republic of China*
[c]*Canyons Worldwide, P.O. Box 86492, Tucson, AZ 85754, USA*
[d]*Lanzhou Institute of Geologic Survey, Lanzhou 730050 Gansu, People's Republic of China*

Received 28 May 2004; revised 5 November 2004; accepted 25 March 2005

Abstract

Geologic mapping in the eastern Himalayan syntaxis confirmed the three regional tectonic elements outlined by previous geologic workers. Our studies, however, show that the Indus-Yarlung Tsangpo suture (IYS) is a continuous mélange zone that forms an inverted U in map view around the Namche Barwa antiform. The Namche Barwa and Nyainqentanglha crystalline complexes lie below and above the IYS suture, respectively, and both were parts of the northern Indian plate basement rocks with petrologically and geochronologically correlative protoliths. Both units were deformed, metamorphosed and intruded at the end of the Proterozoic. The Zhibai Formation, the lower part of the Namche Barwa Group, extends along the northwest slope of the Himalaya, and is mainly composed of highly deformed aluminous felsic gneiss containing sporadic boudins of high-pressure granulite in the Namche Barwa antiform. The upper part of the Namche Barwa Group includes a calcareous rock assemblage characteristized by marble and diopside-bearing calcsilicate rocks interlayed with felsic gneiss. Petrochemical studies show that the IYS contains lenses of oceanic crustal rocks originated from fore-arc trench, island arc, and back-arc basin environments, which implies they were derived from a SSZ-type (supra-subduction zone) ophiolite. Our field mapping identifies the Jiali-Parlung Tsangpo remnant suture (JPS) that lies north of the Namche Barwa antiform as a possible branch of the Neo-Tethyan oceanic realm. Subduction of the Mesozoic Neo-Tethyan oceanic plate resulted in both Mesozoic and Cenozoic granite intrusions in the northwest-trending Gangdise magmatic belt along the southern edge of Asia. Uplift and exhumation have been the most recent dominant tectonic processes in the late Cenozoic for the High Himalayan crystalline rocks (Namche Barwa Group) in the core of the Namche Barwa antiform.

1. Introduction

The Himalayan orogen is one of the youngest mountain belts on Earth created by continent–continent collision and offers an unique opportunity for understanding the process of mountain building (Yin and Harrison, 2000; Zhang et al., 2004). The eastern Himalayan syntaxis has attracted the attention of many geologists for its special tectonic position at the end of the mountain belt expressed as a large antiform, the Namche Barwa antiform. The structure is cored by high-grade metamorphosed rocks, locally formed at high pressure. Higher tectonic units wrap around and dip away from the uplifted core in an inverted U-shaped pattern in map view. This, and a similar structure at Nanga Parbat in the western Himalayan syntaxis, characterize the two syntaxes at opposite ends of the Himalaya. Published research in the Namche Barwa region covers its basic tectonic framework, the high-pressure granulite boudins in the High Himalayan crystalline rocks and the exhumation processes of these high grade rocks (Zheng et al., 2003a,b, 1992; Ding et al., 1995, 2001; Zhong and Ding, 1996b;

* Corresponding author. Address: Chengdu Institute of Geology and Mineral Resources, 82/3 No.1 Ring Road (N), Chengdu 610082, People's Republic of China. Tel.: +86 28 8322 6767; fax: +86 28 8323 1706.
E-mail address: cdgquanru@cgs.gov.cn (G. Quanru).

1367-9120/$ - see front matter © 2005 Elsevier Ltd. All rights reserved.
doi:10.1016/j.jseaes.2005.03.009

Burg et al., 1997, 1998; Liu and Zhong, 1997; Zhang et al., 2004). Below, we briefly describe the general lithology of the region and exhibit tectonic models for its development.

1.1. Main lithology and tectonic units

The eastern Himalayan syntaxis is characterized by three major tectonostratigraphic units (Fig. 1). The High Himalayan crystalline rocks of the Namche Barwa Group that form the core of the Namche Barwa antiform in the middle of the syntaxis; it underlies Namche Barwa, the highest peak in the syntaxis. A narrow, 2–10 km-wide zone, here after referred to as the Yarlung-Tsangpo (IYS) shear zone, forms an inverted U around the high grade rocks of the Namche Barwa antiform and consists of highly deformed metasedimentary, and metaigneous rocks. The Gangdise magmatic belt and associated wall rocks lie to the west, north and east of the IYS shear zone (Zhang et al., 1992). Although there is some structural slivers of rocks of the Namche Barwa Group and the Gangdese belt within the Yarlung-Tsangpo shear zone, the shear zone forms a clearly defined unit bounded by ductile shear zones that separate it from the two more extensive units on either side. The Yarlung-Tsangpo shear zone can be traced to the southwest into the Yarlung-Zangpo suture zone. However our mapping suggests the suture zone has been modified by structures related to formation of the Namche Barwa antiform.

Previous workers subdivided the Namche Barwa antiform into several formations (e.g. Zheng and Chang, 1979; Zheng et al., 2003a,b; Zhang et al., 1992), but did not present an accurate geologic map to illustrate the spatial distribution. Both Zheng et al. (2003a,b) and Zhang et al. (1992) also pointed out that the Yarlung-Tsangpo shear zone (IYS) could be traced into Indus-Yarlung Tsangpo suture, but they did not show accurately its geographic distribution, structural characteristics or lithologic composition due to insufficient field observations.

1.2. Models: crustal folding and exhumation process

The eastern Himalayan syntaxis is an antiformal structure that was developed during Cenozoic India-Asia collision. Burg and Podladchikov (2000) proposed that the antiform developed by lithospheric folding. In contrast, Zeitler et al. (2001) suggested that the antiform was created by upward movement of a high-grade moble core involving only crustal rocks. The uplift could have begun after late Miocene time as a result of duplex development (Ding et al., 2001). The exhumation rate of the antiformal core is $\sim 10\ \mathrm{mm\ yr^{-1}}$ since ~ 4 Ma possibly caused by erosion coeval with crustal-scale folding (Ding et al., 1995; Burg and Podladchikov 2000). The exhumation and cooling history resembles the evolution of Nanga Barbat at the western Himalayan syntaxis in Pakistan (Ding et al., 1995; Zhong and Ding, 1996b; Burg et al., 1997, 1998).

Previous geologic studies dominantly focused on the northwestern part of the antiformal core in order to study the high-pressure metamorphism and exhumation rate of these deeply buried rocks. However, no detailed map of the area was produced to better understand the basic lithologies, structure and tectonic units. No accurate and better constrained interpretations of this complex area was therefore possible.

2. Methodology

During the summers of 2000 and 2001, fieldwork by 25 geologists from the Chengdu Institute of Geology and Mineral Resources and the Gansu Geologic Survey Institute produced a new map of the area at a scale of 1/250,000. The map covered an area of 16,522 $\mathrm{km^2}$ bounded between 94°30′E and 96°00′E in longitude, and 29°00′N and 30°00′N in latitude. Geo-traverses of $\sim$2300 km were made, $\sim$180 km of sections of major lithologies were measured, and more than 1500 samples were collected. A Garmin GPS 12XL personal navigator was used to determine the location of geologic boundaries, samples and field data locations. GPS locations are accurate to $\pm$10–25 m depending on the local topography. Topographic maps at 1:100,000 scale were used for field mapping. Mosaics of LANDSAT-5 TM images over this region were printed at 1:100,000 scale, mosaiced and used in concert with the topographic maps. Prior to our mapping, Chinese geologists had conducted field investigations since the 1980s and submitted several internal Institute reports and maps (Diao et al., 1989; Zhu et al., 1995; Pan et al., 2005). Here we present our map that makes some major advances relative to earlier geologic studies. We include more detailed tectonic outlines and lithologies, and develop a more constrained regional geological evolution. In addition we also present the Jiali-Parlung Tsangpo remnant suture (JPS) north of the main Namche Barwa antiform.

3. Rock units of the Namche Barwa antiform: Subdivisions of the Namche Barwa group (An∈*nj*)

The High Himalayan crystalline in Namche Barwa was described as ‘unidentified migmatite’ and marked as ‘M’ on previous geologic map (Liu, 1986). Although limited field work and geochemical and geochronoligic analyses have been done on high-pressure granulite boudines, the High Himalayan crystallines, refered to as Namche Barwa Group by Zhang et al. (1992), still lacked detailed subdivision prior to this study. Our fielding mapping reveals that the high-pressure granulite boudines occur in a northeast trending zone along the northwest slope of the Himalayas.

The Namche Barwa Group forms the core of the Namche Barwa antiform, the structurally lowest of the three major tectonic units in the area; it is tectonically overlain by

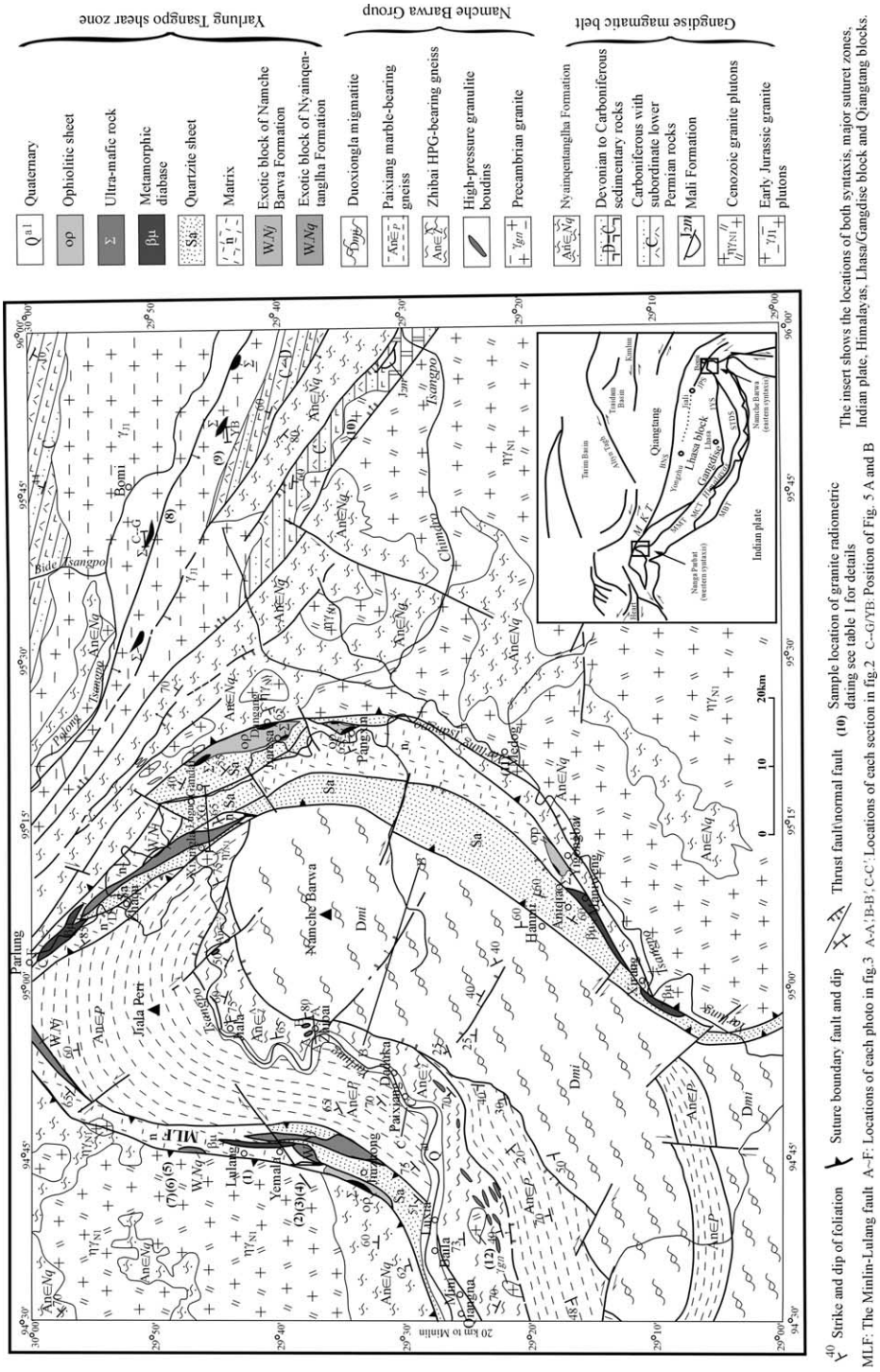

Strike and dip of foliation
Suture boundary fault and dip
Thrust fault\normal fault
(10) Sample location of granite radiometric dating see table 1 for details
The insert shows the locations of both syntaxis, major suturet zones, Indian plate, Himalayas, Lhasa/Gangdise block and Qiangtang blocks.
MLF: The Minlin-Lulang fault A–F: Locations of each photo in fig.3 A-A',B-B',C-C': Locations of each section in fig.2 C–G/YB: Position of Fig. 5 A and B

Fig. 1. Geologic map of Yarlung Tsangpo Grand Canyon.

the Yarlung-Tsangpo shear zone (IYS), which in turn is tectonically overlain by the Gangdise magmatic belt and its wall rocks. The Namche Barwa Group lies within the inverted U-shaped loop formed by the Yarlung-Tsangpo shear zone, and has a mean composition of felsic gneiss. It is subdivided into three mappable lithological units based on rock type and characteristics of the metamorphism and deformational fabrics (Figs. 1 and 2). The rocks of the Namche Barwa Group can be followed south of the map area where they are continuous with the rocks of the High Himalayan crystalline zone.

3.1. Zhibai complex (An∈Z)

The Zhibai complex crops out mainly in the northwestern part of the Namche Barwa antiform adjacent to the big bend in the Yarlung Tsangpo River (Fig. 1). Rocks of the Zhibai complex (An∈*Z*) are the most highly metamorphosed and have undergone the highest-temperature ductile deformation of all the units in the antiform (Fig. 2). It is composed of aluminous felsic gneiss with sporadic pockets of garnet clinopyroxenite, garnet amphibolite and kyanite garnet monzogneiss (Fig. 3A and B). These 'high-pressure granulite' lenses record peak metamorphic conditions of $T=720$–760 °C and $P=0.8$–1 GPa according to Burg et al. (1998), or $T=750$–890 °C, $P=1.4$–1.8 GPa, corresponding to a depth about 50–60 km according to Zhong and Ding (1996a), Liu and Zhong (1997, 1998) and Ding and Zhong (1999). U/Pb radiometric ages of zircons extracted from a garnet clinopyroxenite in the Zhibai complex were dated at 1312 ± 16 Ma and those from a metapelite yielded an age of 1770 Ma (Burg et al., 1998). This could be the age of the protolith and is similar to protolith ages of 1850 Ma in the Nanga Parbat region (Zeitler et al., 1993; Winslow and Zeitler, 1996). $^{40}Ar/^{39}Ar$ cooling ages of 42.67 ± 2.54 Ma and 35.73–82.89 Ma were determined from hornblende and clinopyroxene, respectively. Ding et al. interpreted that peak metamorphism for these rocks occurred between 45–69 Ma (SHRIMP Zircon U/Pb ages from kyanite garnet gneiss are 44.5 ± 4.93 Ma, 60.9 ± 1.95 Ma, 65.69 ± 1.53 Ma, 68.57 ± 1.70 Ma; clinopyroxene $^{40}Ar/^{39}Ar$ age from garnet clinopyroxenite yielded an age of 64.56 ± 1.29 Ma. Ding and Zhong, (1999). Ding et al. interpreted the SHRIMP Zircon ages at ~40 Ma from mafic granulite to have crystallized in the presence of fluids associated with high-pressure granulite facies metamorphism (Ding et al., 2001).

3.2. Duoxiongla migmatite (Dmi)

The Duoxiongla migmatite is composed of migmatitic gneiss, augen gneiss and banded gneiss, and crops out over a large area in the eastern part of the Namche Barwa antiform (Figs. 1 and 2). It consists of plagioclase and quartz along with biotite and hornblende, with rarer amounts of garnet than in the Zhibai complex (An∈*Z*) and scarce K-feldspar and sillimanite. There was no age data for the protolith of D*mi* until now. Burg et al (1997, 1998) studied the felsic bands in migmatitic gneiss near Duoxiongla and concluded that migmatization occurred between 3.3–3.9 Ma. His data yielded exhumation rates in this region of 10 mm y^{-1} at 3.2–3.3 Ma and 3–5 mm y^{-1} at ~2.2 Ma.

3.3. Paixiang formation (An∈P)

The Paixiang Formation is dominantly a felsic gneiss with subordinate diopside and forsterite-bearing marble, clinopyroxenite, and scapolite diopsidite (Fig. 2). It exhibits compositional layering and chevron and kink folds locally in contrast to the more ductile folding in the Zhibai and Duoxiongla migmatite units, which suggests that the Paixiang Formation represents a structurally higher part of the High Himalayan crystalline rocks.

The Duoxiongla migmatite may have resulted from Cenozoic migmatization of the Zhibai complex and Paixiang Formation according to its field distribution and main lithologic component of banded felsic gneiss with subordinate amphibolite and metamorphic characteristics. One alternative explanation is that it was originally a middle unit between the upper Paixiang Formation and the lower Zhibai complex.

These three lithologic units are bounded by ductile strike-slip faults and steep normal faults against the Yarlung Tsangpo shear zone. Our mapping also recognized several Early-Paleozoic granite intrusions in the Namche Barwa Group with U–Pb zircon ages of 525–552 Ma (Pan et al., 2005, Fig. 1). These data, coupled with the old protolith ages mentioned above, support the correlation of the Namche Barwa Group as the eastern continuation of Precambrian High Himalayan basement rocks.

4. Lhasa and bomi blocks/the gangdise magmatic belt

The region to the west, north and east of the narrow Yarlung-Tsangpo shear zone is formed by the Lhasa and Bomi blocks. These two blocks were both considered as the Lhasa block until our mapping demonstrated they are separated by a narrow suture zone, the Jaili-Parlung-Tsangpo suture zone (see below). Both the Lhasa and Bomi blocks (refered to as Transhimalayan terrain by Gansser, 1964 and Burg et al., 1998 in this region are mainly composed of Precambrian basement rocks (Nyainqentanglha Group, An∈*Nq*), Paleozoic and Mesozoic cover strata intruded by abundant Mesozoic and Cenozoic granitic plutons (Fig. 4).

4.1. The Nyainqentanglha Group (An∈Nq)

The Nyainqentanglha Group is mainly composed of banded migmatite, biotite felsic gneiss and augen granitic gneiss, along with sporadic marble lenses. It has yielded radiometric protolith ages of 1453–2296 Ma (Zhu et al., 1995, internal report) and is considered the basement rocks

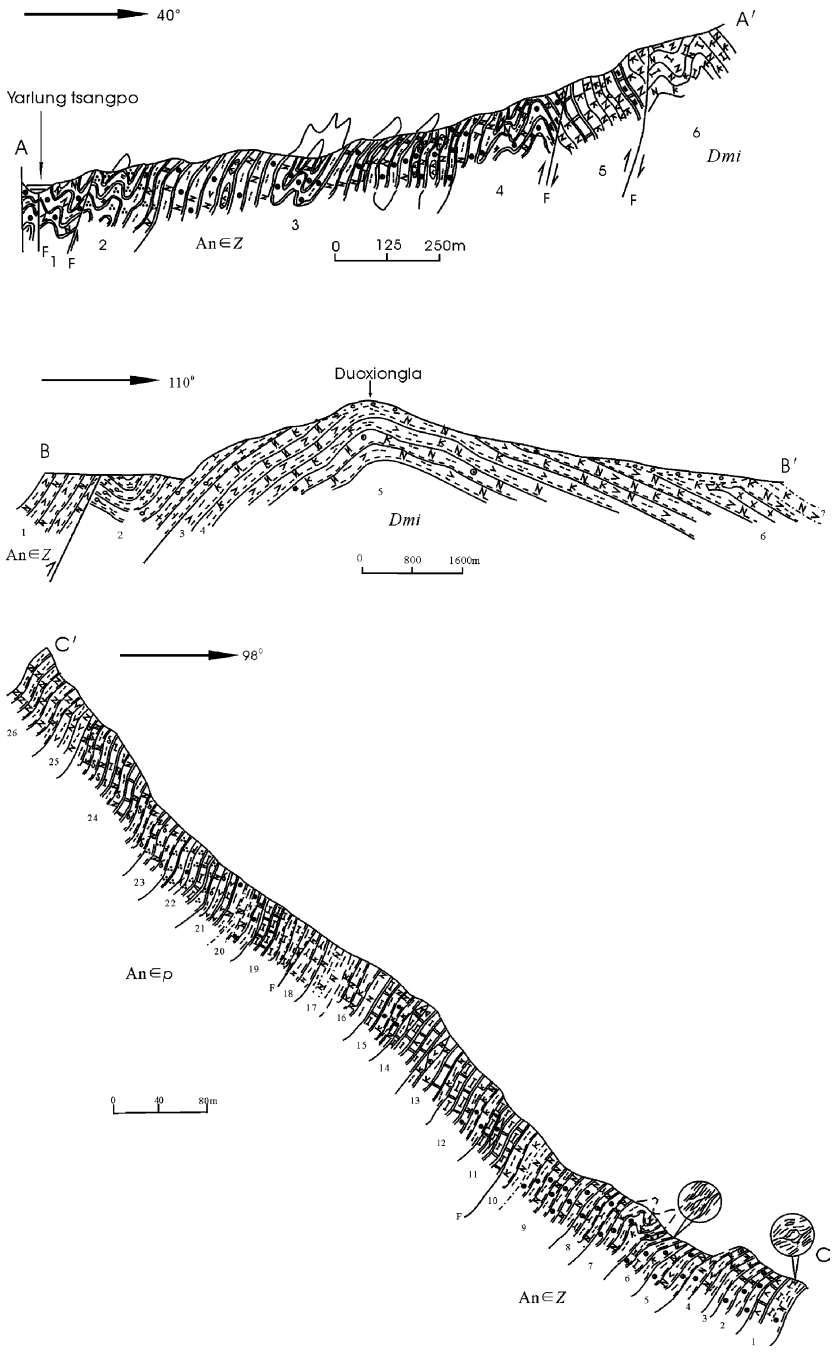

Fig. 2. Geologic sections of the Namche Barwa Group (see Fig. 1 for locations). Section A∼A′ Measured geologic section in the Bulong valley. (1) Strongly mylonized kyanite-bearing garnet plagioclase gneiss; (2) garnet biotite plagioclase gneiss with diopside plagioclase amphibolite lens (HP granulite); (3) biotite quartz schist, amphibolite and two mica plagioclase gneiss; (4) sillimanite garnet gneiss with garnetamphibolite lens (HP granulite); (5) two feldspar granulite and plagioclase gneiss with marble interbeds; (6) Duoxiongla migmatite, contact with the above Zhibai Formation by a mylonite zone. Main rock type is grey two feldspar migmatite. Section B∼B′ Freehand geologic section across the Duoxiongla migmatite. (1) Garnet hornblende gneiss with HP granulite lens; (2) banded granitic gneiss; (3) biotite two feldspar gneiss; (4) hornblende biotite two feldspar gneiss; (5) biotite plagioclase gneiss, biotite two feldspar gneiss and garnet biotite two feldspa gneiss; (6) hornblende biotite plagioclase gneiss with diabase vein. Section C∼C′ Measured section across the Zhibai and Paixiang Formations. 1–10) strong ductilly deformed rocks of the Zhibai Formation: garnet biotite two feldspar gneiss, garnet sillimanite hornblende plagioclase gneiss with HP granite lens (garnet clinopyroxenite, garnet sillimanite two feldapar gneiss); 1126) Paixiang Fomation in contact with the above Zhibai Formation by a mylonite zone. Major rock types are biotite plagioclase gneiss, graphite diopside marble, olivine marble, banded biotite hornblende plagioclase gneiss, etc.

for the Lhasa and Bomi blocks. Previous workers have suggested that the Precambrian Higher Himalaya crystalline in the east and west syntaxes and the basement rocks for the Gangdise magmatic belt have similar lithologies and protolith ages (Chamberlain et al., 1991; Tahirkheli, 1996; Xia and Liu, 1997) and represent the basement rocks for the passive northern margin of Gondwana supercontinent in Paleozoic time.

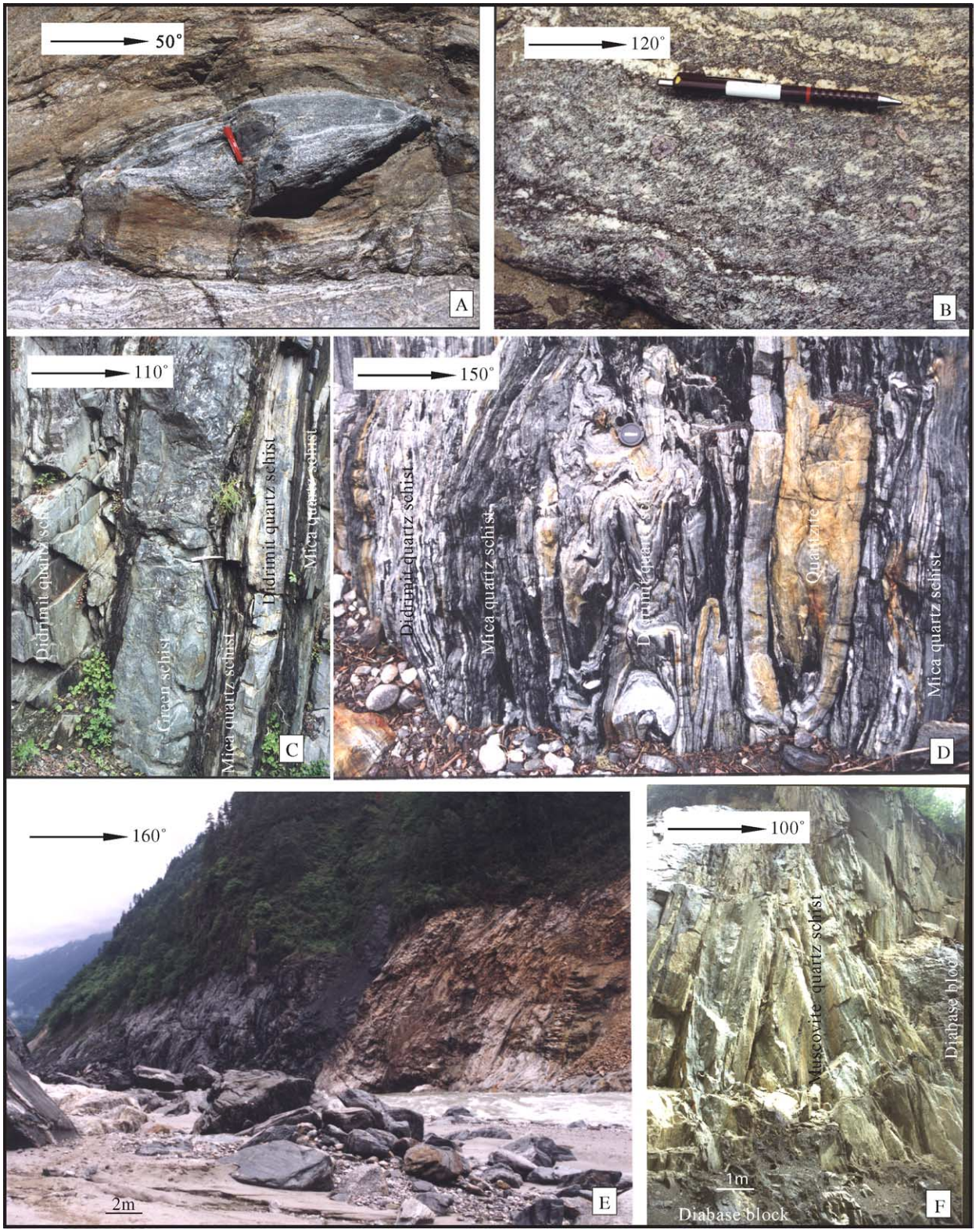

Fig. 3. Main rock types of the Zhibai complex (A and B) and dominant components of the IYS mélange zone (C–F). (A) Felsic gneiss containing kyanite garnet gneiss boudins, lower part of Namche Barwa Group. (B) highly-deformed felsic gneiss with 'S–C' fabrics, lower part of the Namche Barwa Group. Both A and B were collected in the valley of Bulong located ~1 km north of Zhibai. B was collected in the shear zone close to the contact between the D*mi* and An∈Z. (C) Interbedded mica quartz schist and greenschist with blastopillow structure located ~2 km south of Parlung. (D) Thin-layered quartzite and mica quartz schist are strongly deformed and tightly folded located ~1.5 km north of Zhaqu. (E) A 200-m-wide panoramic view of a palimpsest diabase dike (a block in mélange) and mica quartz schist (matrix) with sharp contacts located ~8 km north of Zhaqu. (F) Muscovite quartz schist with 2-phased sharp vertical folds. Dark-colored rocks are small metamorphosed diabase blocks located ~2 km east of Parlung. See Fig. 1 for locations of each photo.

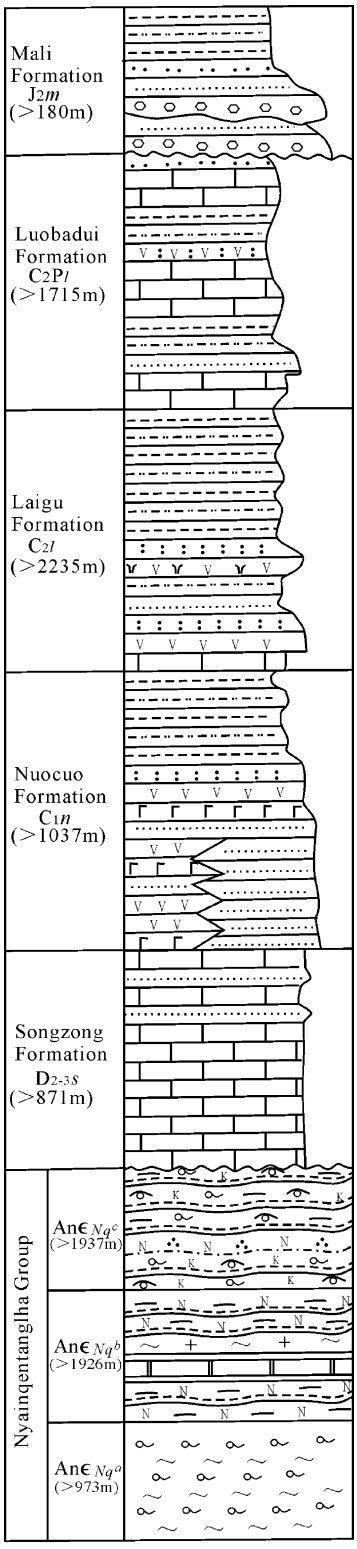

Fig. 4. Columnar section of the Gangdise arc zone. Figures in brackets are measured thicknesses. An∈Nq^a = banded migmatite and biotite felsic gneiss; An∈Nq^b = felsic biotite gneiss and migmatite with marble beds; An∈Nq^c = mylonite and K-feldspar gneiss; $D_{2-3}s$ = marble with meta quartz sandstone; C_1n = meta sandstone, slate with andesite, basalt and dacite interbeds; C_1l = meta sandstone, slate with andesite and limestone interbeds; C_2Pl = thick limestone, slate and sandstone with minor andesite interbeds; J_2m reddish diamictite conglomerate, siltstone and slate.

4.2. Paleozoic and mesozoic cover rocks

The sedimentary cover of the Nyainqentanglha Group consists of Devonian to Jurassic sedimentary rocks along with volcanic intercalations at the northeast corner of this region. The Paleozoic sedimentary section above the Nyainqentanglha Group includes the Devonian Songzong Formation ($D_{2-3}s$), the lower Carboniferous Nuocuo Formation (C_1n), the upper Carboniferous Laigu Formation ($C_2 l$) and the upper Carboniferous to lower Permian Luobadui Formation (C_2Pl) (Figs. 1 and 4). Marine diamictites and sporadic faceted stones in pebbly mudstone in the Carboniferous and Permian strata north and east of the map area are of glacial origin and indicate that the Lhasa and Bomi blocks were parts of the late Paleozoic Gondwana sequence (Hsu et al., 1995).

Thick carbonate deposits of the D_{2-3} *s* suggest a typical stable shallow marine shelf (Xia and Liu, 1997), which was followed in early Carboniferous time by an influx of terrestrial clastic sediment containing large amount of volcanic material (C_1n) composed of andesite, basalt and dacite. These sedimentary and volcanic strata were unconformably overlain by the Mali Formation of middle Jurassic age. The Mali Formation is exposed only in the valley of Langqiu to the east of the region (Fig. 1). It overlies the Luobadui Formation (C_2Pl) unconformably and is thrust over by the Nuocuo Formation (C_1n). The main rock types of the Mali Formation J_2m are reddish conglomerate, sandstone, sandy mudstone and siltstone with subordinate thin layers of purple and green dacite tuff, which suggest a continental environment.

4.3. Magmatic rocks of the Gangdise belt

The Gangdise granitic plutons are present west, north and east of the Yarlung-Tsangpo shear zone, but only rarely intrude the shear zone and the Namche Barwa Group in the core of the antiform. The abundant plutons that intrude the Nyainqentanglha basement rocks and their Paleozoic and Mesozoic cover rocks form the Gangdise magmatic belt of the Lhasa and Bomi blocks. Mapping the distribution of these plutons was aided by satellite imagery. The ages of these plutons are from our new radiometric data and also from published papers (Table 1 and Fig. 1).

The Gangdise magmatic arc is known for its abundant Mesozoic and Cenozoic volcanic rocks in the western and middle parts of the Himalaya Liu, 1988; Pearce and Mie, 1985. In the map area, however, the arc consists of dominantely intrusive rocks. These Mesozoic plutons occur as large batholiths that have a general NW-SE trend on both sides of the Jiali-Parlung Tsangpo suture zone (see below) that separates the Lhasa and Bomi blocks. They yield radiometric ages of 227 to 69 Ma (Table 1). A common explanation for the genesis of Mesozoic plutons is that they resulted from the subduction and closure of the Bangong-Nujiang Tethys during the Mesozoic (Pan et al., 1997; Geng et al., 2001). Some Cretaceous plutons close to

Table 1
Radiometric ages of granite plutons

Location	Rock type	Ages/Ma	Methods	Mineral	References	Locations on Fig. 1
N. Sheqila	Tonalite	17±0.3	$^{40}Ar/^{39}Ar$	Bi	This study	(1)
S. Sheqila	Granite	17.3±0.4	$^{40}Ar/^{39}Ar$	Bi	This study	(2)
S. Sheqila	Granite	18.1±0.4	$^{40}Ar/^{39}Ar$	Mu	This study	(3)
S. Sheqila	Granite	17.1±0.5	$^{40}Ar/^{39}Ar$	Bi	This study	(4)
Dongjiu	Granodiorite	14±0.3	$^{40}Ar/^{39}Ar$	Bi	This study	(5)
Dongjiu	Tonalite	13.6±0.3	$^{40}Ar/^{39}Ar$	Bi	This study	(6)
Dongjiu	Quartz diorite	14.3±0.3	$^{40}Ar/^{39}Ar$	Bi	This study	(7)
Soxinongba	Granite	74.24±1.48	$^{40}Ar/^{39}Ar$	Kf	This study	(9)
Jiangbietang	Quartz diorite	79.43±1.34	$^{40}Ar/^{39}Ar$	Pl	This study	(10)
Dexing	Pegmatite	94.32±1.07	$^{40}Ar/^{39}Ar$	Pl	This study	(11)
Luxia	Gneissic granites	553–525	U/Pb	Zircon	Pan et al. (2005)	(12)
Galongla	Granodiorite	69–104.3	U–Pb	Zircon	Burg et al. (1998)	(8)
Dongjiu	Granite	15.9±0.19	$^{40}Ar/^{39}Ar$	muscovite	Ding et al. (2001)	
Zhibai	Granulite	17.5±0.30	$^{40}Ar/^{39}Ar$	hornblende	Ding et al. (2001)	
Daduka	gneiss	7.9±0.18	$^{40}Ar/^{39}Ar$	hornblende	Ding et al. (2001)	
Tongmai	mylonite	11–25	SHRIMP	Zircon	Ding et al. (2001)	
Zhibai	Granulite	~40	SHRIMP	Zircon	Ding et al. (2001)	
Zhibai	Granulite	~65	SHRIMP	Zircon	Ding et al. (2001)	
Zhibai	Granulite	~160	SHRIMP	Zircon	Ding et al. (2001)	
Duoxiongla	Gneiss	484.1±2.4	U/Pb	Zircon	Burg et al. (1998)	
Zhibai ~ Duoxiongla	gneiss	0.9–8.2	Fission track	Apatite, zircon	Burg et al. (1998)	

the Yarlung-Tsangpo suture are related to northward subduction in the IYS Neo-Tethyian ocean during late Mesozoic time. Cenozoic granitic rocks underlie large areas NW and SE of the map region (Fig. 1) and may be the most abundant magmatic rocks in the Gangdise arc. Petrochemical and radiometric studies suggest that they resulted from crustal partial melting during the late stage of the India-Asia collision and post-collisional crustal melting.

4.4. Inner arc rift zone

4.4.1. The Jiali-Parlung Tsangpo suture (JPS)

The Jiali-Parlung fault has been described as a Cenozoic dextral strike-slip fault to the north and east of the Assam-Namche Barwa syntaxis (Ratschbacher et al., 1995; Holt and Wallace, 1991). Geologic mapping revealed that it is also a remnant ophiolite-bearing zone. Ultramafic and mafic lens or blocks are sporatically present in a narrow zone (1–3 km wide) within the Gangdise arc along the eastern continuation of the Jaili fault zone northeast of the Namche Barwa antiform (Fig. 1). These lenses and blocks trend WNW (300°). Along the same trend are lenses and blocks of marble and banded chert enclosed and intruded by the Mesozoic Gangdise granitic batholiths (Figs. 1 and 5). Two representative cross sections, out of five such exposures of these rocks, are presented in Fig. 5. Zhu et al. (1995) have documented this suture as a 'zone of ultramafic rocks' in their internal report of geologic mapping in Bomi, but they did not interpret it as an inner arc ophiolitic mélange. These blocks are often more than 100 m long, but most of them are 1–10 m long. They were metamorphosed to greenschist facies and strongly deformed. Deformation of some blocks and diabase dikes could reflect structural movements before granite intrusion in the Mesozoic (Fig. 5B). Geochemical studies suggested that these mafic and ultramafic blocks were parts of a dismembered ophiolite suite and originated in an inner-arc rift basin during the Mesozoic. This zone, the Jaili-Parlung-Tsangpo (JPS) suture, is interpreted to separate what was previously considered a single Lhasa block into two parts, the Lhasa and Bomi blocks to the SW and NE, respectively.

The JPS is the eastern continuation of a northwest- trending ophiolitic mélange belt refered to as the Yongzhu-Namucuo-Jiali rift zone within the Gangdise tectonic domain, which has been confirmed by geologic mapping in recent years. More exposures of a relatively complete ophiolite suite have been found within what is considered to be the extension of this zone around Yongzhu (Yang et al., 2003; Wang et al., 2003). The age of the JPS ophiolite has not yet been determined. Stratigraphic and zircon U–Pb radiometric constraints on the mafic and ultramafic rocks around Yongzhu yield ages of late Jurassic to early Cretaceous (Yang et al., 2003; Wang et al., 2003). However, the ultramafic and mafic rock blocks in Chuangba (Figs. 1 and 4), a mountain pass about 5 km south of Bomi, yield a Rb–Sr radiometric age of 215±63 Ma (Zhu et al., 1995, internal report). Obviously these data may be unreliable as representing the original age of the ophiolite within the JPS zone. We interpret the Jiali-Parlung Tsangpo remnant ophiolitic mélange as a Mesozoic inner-arc rift zone, but more geologic and geochronologic studies are necessary to support this interpretation.

5. Eastern segment of the Yarlung-Tsangpo suture: the Yarlung-Tsangpo shear zone (IYS)

The Yarlung-Tsangpo suture zone can be traced continuously into the eastern Himalayan syntaxis where it forms the middle tectonic unit separating the core of the Namche

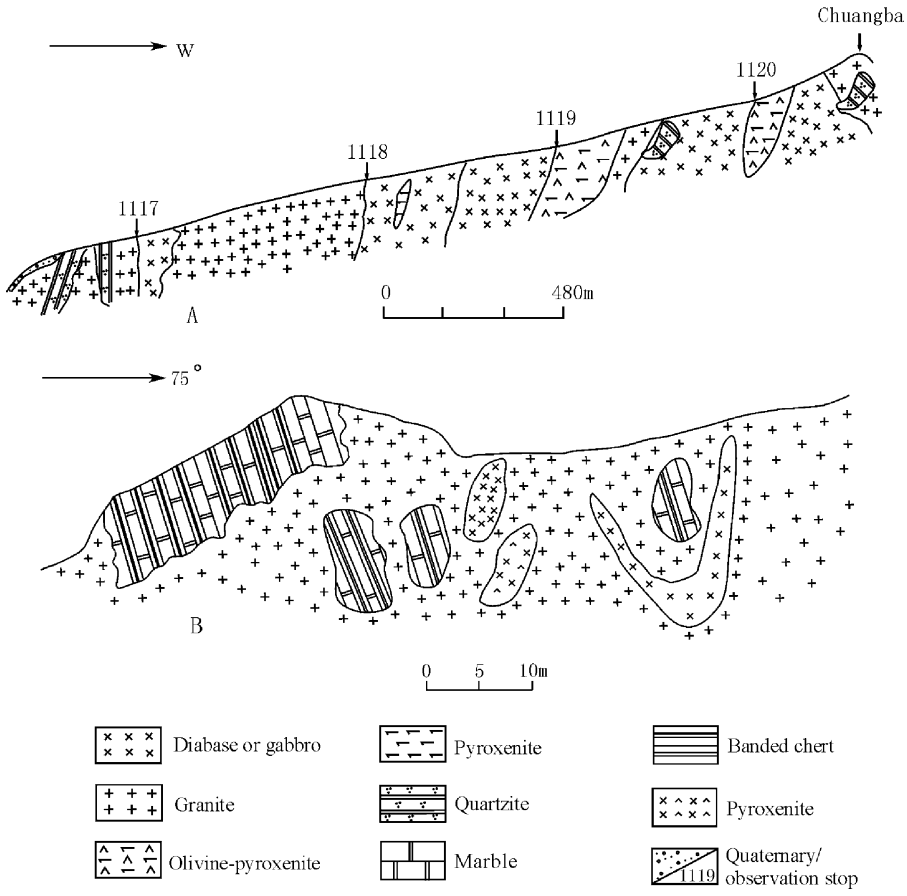

Fig. 5. (A) Geological cross section from Ganong to Chuangba (C–G on Fig. 1). (B) Exposures in Yaba valley (YB on Fig. 1). Both exposures contain blocks of mafic and ultramafic rocks in the Jiali-Parlung Tsangpo ophiolitic mélange.

Barwa antiform from the Lhasa block/Gangdese arc tectonic units. It was formerly shown to be offset by the sinistral Milin-Lulang fault and the dextral Aniqiao fault for about 60 km (Zheng et al., 2003a,b; Zhang et al., 1992; Burg et al., 1998), due to intensive northeast indentation of the Indian plate (Liu et al., 2000). Ding et al. (2001) interpreted the northwest boundary fault as a folded thrust. Our field mapping, however, has revealed that it is a 2–10 km wide continuous zone of sheared rocks, containing ophiolitic fragments, that forms an inverted U-shaped zone defining the north-plunging Namche Barwa antiform. The northwestern-most part of this zone remains poorly exposed (Fig. 1).

The well-documented south Tibet detachment (Burchfiel et al., 1992) to the west is difficult to identify in this region because there are no northern Himalayan sedimentary rocks on top of the high Himalayan crystalline rocks. However our field work and study of satellite images suggested that the STD may join the folded IYS shear zone around the village of Nanyi ~2 km west of Milin, but this interpretation needs more evidence.

5.1. Boundary faults of the IYS zone

The Milin-Lulang fault is actually a fault zone with two faults along both sides of the IYS (Fig. 1). The northwest fault is referred to as the Milin-Yanggudajue-Lulang-Parlung fault, which divides the IYS mélange in the footwall from the Lhasa block and Gangdise arc to the northwest in the hanging wall. The boundary fault on the southeast side, the Luxia-Dadingbigong fault, separates the IYS from the Namche Barwa Group on the southeast side. Both faults are intensively mylonitized shear zones, which can be easily traced in the field and by examining satellite images. The best outcrops of mylonitic rocks is on the north side of the Gangga bridge, near Milin. The orientation of asymmetrical augen metacrysts here indicate sinistral shear. The overprinted down-dip lineations on the foliation planes may suggest down-to-the-west detachment faulting at a later stage.

The eastern part of the IYS zone is much wider, and contains more ophiolitic rocks (Fig. 1). Its boundaries on the west and east sides are formed by the folded Hanmi-Xixing-la and Medog-Parlung faults, respectively. The well-documented Aniqiao mylonite zone crops out along the SE segment of the IYS and is characterized by fine-grained 'high-grade mylonite' composed of felsic, aluminous, mafic and marble-dominated mylonites (Zhang et al., 1992; Wang, 1993). This continuous mylonite zone can be traced NE and NW for ~150 km, and can also be easily recognized between Xixingla and Guodeng and to the northern tip of the Namche Barwa massif. The Medog-Parlung fault along

the eastern boundary of the IYS could not be easily identified in the field by its petrologic contacts or structural deformation due to thick vegetation and granite intrusions, but was clearly identifiable on remote sensing images.

The boundary faults are concordantly folded and outline the western and eastern sides of the Namche Barwa antiform. They may join each other in the north at the north-plunging tip of the antiform, as do similar faults in the western Himalayan syntaxis (Zeitler et al., 2001). We interpret them as strike-slip shear zones that accommodated the northward indentation of the folded Indian plate at an early stage of the India-Asia collision. However, in some places, such as at Dadingbigong south of Dongjiu in the northern part of the region and in the valley ~2 km east of Parlung, these ductile fault zones are overprinted by normal fault breccia zones that follow present-day valleys. The normal displacement may reflect late stage detachment faulting and rapid exhumation of the rocks of the antiform as described by Burg et al (1997, 1998) and Ding et al (1995, 2001). Evidence in the IYS zone for differential extensional uplift of the antiform include ubiquitous asymmetrical augen metacrysts, asymmetrical small folded quartz veins and extensional down-dip lineation on foliation plains. About 1.5 km north of Jiaresa, two groups of lineations are present where a roughly horizontal lineation was overprinted by a younger and better developed vertical lineation representing the two kinematic events.

5.2. Major lithologic units in the IYS shear zone

Our field studies show that basic components in the IYS shear zone are greenschist, mica-quartz schist and various lenses of a dismembered ophiolitc suite (Fig. 3), an assemblage of rocks that are easily distinguishable from the Namche Barwa Group and the Lhasa block/Gangdise arc units that lie structurally below and above respectively. Ultramafic and mafic lenses in some places coexist with blastobasalt pillow lava and quartzite to form relatively complete ophiolitic sequences (marked as 'op' in Fig. 1). We also recognized mappable exotic felsic gneiss and marble lenses in the IYS zone, which may have initially come from Precambrian basement rocks from the tectonic units above or below the IYS zone. The lenses of different rock types are of variable size and lie within what we consider a matrix of greenschist and mica-quartz schist in the IYS shear zone. These rocks can be interpreted as an original belt of mélange (Geng et al., 2004). The contact between the rock lenses and matrix, and the IYS shear zone and adjacent rocks, are formed by faults and mylonite zones. The cross strike measured geologic section presented in Fig. 6 illustrates the major components and structural characteristics of the IYS mélange.

5.3. Petrochemistry and supra-subduction zone ophiolite

Petrochemical and trace element studies on the IYS dismembered ophiolitic rocks suggest a back-arc basin affinity, which is comparable to similar rocks within the IYS suture zone at Xigatze and Zedang (Hao et al., 1999; Geng et al., 2000; Zhang and Zhou, 2001). This back-arc basin was interpreted by Hsu et al. (1995) and Pan et al. (1997) to have been initiated by southward subduction within the Bangong-Nujiang ocean which closed in the late Mesozoic. The IYS back arc basin is referred to as part of the Neo-Tethys that existed from Late Triassic to Eocene time and was the locus of northward subduction beginning in Cretaceous time. We interpret the ophiolitic rocks in the IYS suture zone be fragments of back arc oceanic crust of the Neo-Tethys.

Petrologic studies on the metamorphosed ultramafic and mafic rocks in this region further confirm their SSZ-type ophiolite (supra-subduction zone ophiolite, Pearce et al., 1984) affinity (Hao et al., 1999; Zhang and Zhou, 2001; Geng et al., 2004).

Detailed petrochemical studies from the lenses in the IYS shear zone reveal different genetic settings across a magmatic arc system: (a) Boninites around Pangxin and Jiaresa in the eastern part of IYS shear zone suggest a fore-arc trench environment (Hickey and Frey, 1982; Sobolev and Danyushevsky, 1994; Zhang and Zhou, 2001), (b) Metabasalt samples from Yigongbai and Maniweng, south of Pangxin, show petrochemical similarities to arc tholeiite, (c) Back-arc basin basalts are present in the northern (Parlung-Gandai) and western (Luxia-Yanggudajue) parts of the IYS shear zone. Complete analytical geochemical data and $^{40}Ar/^{39}Ar$ dating data are given in the appendix Tables A1–A4 and in Geng et al. (2000, 2004) more data are available upon request from the authors.

Fig. 7 shows the geochemical transition of meta-basalts in different parts of the IYS shear zone and further confirms our genetic environmental analysis (Geng et al., 2004). Metabasalt samples at Jiaresa-Pangxin have the highest MgO/TiO_2 and lowest $Zr+Y$ values confirming their boninite characteristics (5 in Fig. 7). Meta-basalts samples from the back-arc basin environment have the highest $Zr+Y$ and lowest MgO/TiO_2 values (1, 2 and 6 in Fig. 7). Samples from Yigongbai and Maniweng with low values for both $Zr+Y$ and MgO/TiO_2 are interpreted to be arc tholeiites. The successive compositional transitions of meta-basalts reflecting their affinities with a fore-arc trench, island arc and back-arc basin further indicates that the IYS shear zone in this region includes pieces of oceanic and arc crust and further supports the probable mélange origin for this zone in what was originally a subduction zone setting. The rocks have been strongly deformed from their original positions because of tectonic indentation and orogenesis since the Eocene.

6. Geochronology and tectonic evolution

The region between the Bangong suture to the north and the Yarlung Tsangpo suture has been refered to as Lhasa terrane (Chang and Zheng, 1973; Dewey et al., 1985; Searle et al., 1988; Yin and Harrison, 2000) which separated from

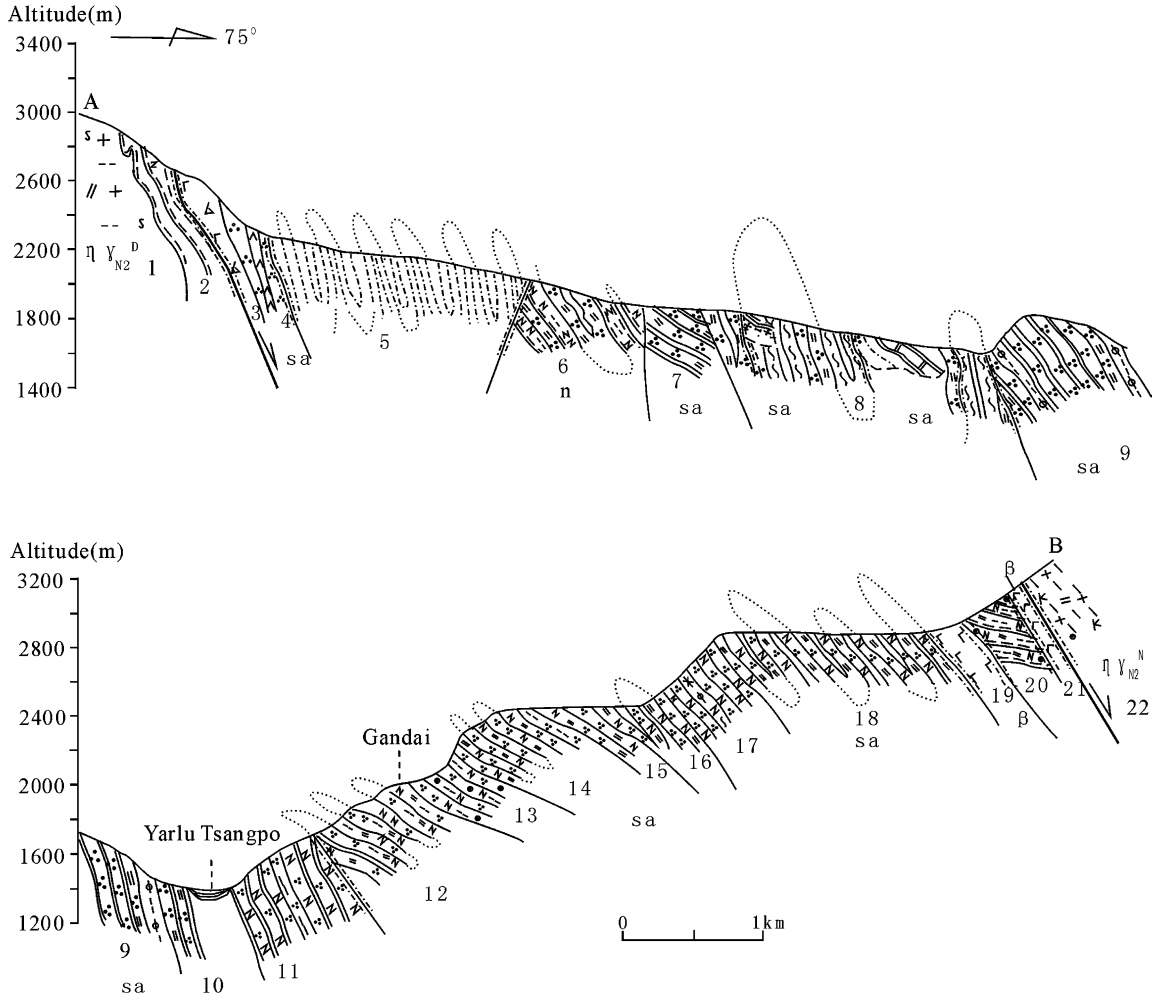

Fig. 6. Geologic section between Xixingla and Gandai (XG on Fig. 1). Dominant lithology of each layer: (1) fine-grained biotite gneissic granite; (2) biotite-bearing two-feldspar gneiss (An∈*nj*); (3) metamorphic breccia-bearing basalt; (4) quartzite schist with amphibole schist; 5) biotite two-feldspar granulite (exotic block of An∈*nj*); (6) amphibole biotite plagioclase gneiss containing muscovite quartz schist; (7) schistose muscovite quartzite; (8) muscovite quartzite schist with blocks of An∈*nj*; (9) quartzitic schist, biotite schist; (10) schistose muscovite-bearing quartzite; (11) feldspar and biotite quartz schist; (12) feldspar two-mica quartz schist; (13) garnet-bearing biotite, feldspar quartz schist; (14) muscovite feldspar quartz schist and biotite quartz schist; (15) muscovite feldspar quartz schist; (16) feldspar quartz schist; (17) feldspar quartz schist and greenschist; (18) muscovite feldspar quartz schist (7–18 are quartz schist layers); (19) amphibolite; (20) garnet plagioclase gneiss (An∈*nq*); (21) amphibolite; (22) gneissic muscovite-bearing granite; sa: quartz schist lenses; n: matrix in the melange belt. Lenses and and matrix have faulted contacts. This is a complete measured section cut spart at layer 9 for convinience of drawing. Granite plutons intruded both ends of the section.

the Indian plate in the late Triassic (Yin and Harrison, 2000). It was believed that the Mesozoic magmatic belt of the Lhasa block was initiated from northward subduction in the Yarlung Tsangpo Neotethyan ocean in middle Cretaceous time. However, as more ophiolitic mélange zones have been found within the Lhasa block (Liu et al., 1988; Yang et al., 2003; Wang et al., 2003) and Late Triassic granite plutons have been identified in recent years (Li et al., 2003), the traditional model for the evolution of the Gandgise and Lhasa block has to be modified. Hsu et al. (1995) proposed a hypothesis based on the archipelago model of orogenesis in order to interpret the tectonic evolution of the entire Tibetan plateau. Based on field observation and the literature, we found that a similar model may be appropriate for our mapping region.

Our geological, petrological and geochronological data combined with unpublished geologic reports and published data (Tables 1 and 2) enable us to present a new and more complete geologic map and propose a tectonic model for the regional geologic evolution of the easteran syntaxial area around Namche Barwa. We propose a four-phase geologic evolution model (Fig. 8).

6.1. Evolution of the north India Precambrian basement

Both the Namche Barwa and Nyainqentanglha Groups have similar protolith ages and correlate with those of the Nanga Parbat area in the western syntaxis (Table 2) (Fig. 8A and B). The granite plutons in the Namche Barwa Group that range in age from 525 to 552 Ma (Pan et al., 2005)

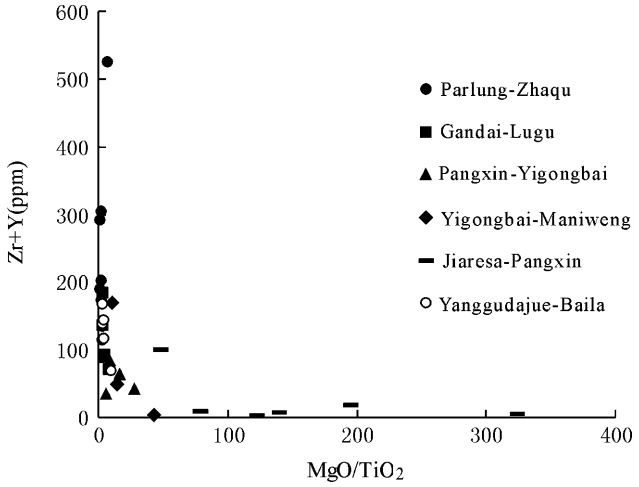

Fig. 7. MgO/TiO_2 vs. (Zr + Y) diagram for meta-basalts.

suggest that the rocks of the northern India plate were intruded and recrystallized at the end of the Proterozoic to form Precambrian basement for younger sedimentary rocks.

Petrological studies revealed the primary sediments of the northern Indian terrain in the Namche Barwa region, the Zhibai complex in the lower part of Namche Barwa Group, are mainly composed of aluminous gneiss and interlayered amphibolite containing high-pressure granulite boudins. Their protoliths, based on geochemical studies, are pelite, sandstone and basic volcanic rocks (Zhang et al., 1992). The upper part of the Namche Barwa Group, the Paixiang Formation, is composed of felsic gneiss, marble and diopside-bearing calcsilicate layers. Geochemical analysis suggest that most of these rocks were pelite, carbonate rocks and calcareous pelite. The Nyainqentanglha Group that form the basement rocks for the Gangdise magmatic arc has similar lithologies, both petrologically and geochronologically, to the Namche Barwa Group. However these rocks occur in the hanging wall of the IYS suture zone and did not experience the high-pressure metamorphism of the rocks below the suture zone.

The northern margin of the Indian plate is interpreted as a Proterozoic basin that contained a thick sedimentary succession with basic volcanic rocks during the Early Proterozoic. The margin evolved into a passive carbonate platform in the Late Proterozoic that was deformed, intruded and eroded to form a landsurface of low relief at the end of the Proterozoic.

6.2. The Late Paleozoic: conversion of the sediment basin

In the central part of the Himalaya, Lower Paleozoic to Mesozoic passive margin sedimentary deposits are well-developed and cover gneissic rocks of the Higher Himalayan crystalline zone (Fig. 8C and D). However, nearly everywhere these two rock groups have been juxtaposed by faults of the South Tibetan detachment zone in Cenozoic time (Burchfiel et al., 1992). We interpret the absence of lower Paleozoic rocks over much of this region to rapid erosion during the Cenozoic. An alternative explanation is that the northern margin of the Indian plate in much of this region was subject to erosion during the early Paleozoic until Devonian time.

The Devonian/Carboniferous (D_{2-3} s/C_1n) contact marks an important transition in this region (Fig. 3). The Songzong Group of Devonion age consists of carbonate rocks that are interpreted to be a typical stable shallow-sea platform sequence (Xia and Liu, 1997). The Nuocuo Group of Early Carboniferous age is composed of clastic deposits with large amounts of interbedded andesitic, basaltic and dacitic volcanic rocks, which suggests that the depositional platform began to break up and subside rapidly in the Early Carboniferous. Rifting and subsidence in northern India reached its deepest levels in the late Carboniferous with the deposition of thick turbidites of the upper Laigu Formation ($C_2 l$). The lower Permian basalts in southern Tibet represent the incipient opening of Neotethys (Garzanti et al., 1999). Our findings may suggest that the northern Indian plate began rifting in early Carboniferous time.

Table 2
Radiometric data in studied region

Location	Rock type	Method	Mineral	Ages/Ma	References
Doxiongla	Biotite-K-feldspar gneiss	U–Pb	Zircon	$484+3,-2$	Burg et al. (1998)
Luxia	amphibolite	Ar–Ar	Hornblende	575.20 ± 5.24	This study
Zhibai-Duoxiongla	Gneiss	Rb–Sr	Isochron	749.38 ± 37.22	Zhang et al. (1992)
Dayandong	Amphibolite	Rb–Sr	Isochron	961 ± 139	Zhu et al. (1995)
Xixingla	Amphibolite	Rb–Sr	Isochron	1064 ± 82	Zhu et al. (1995)
Zhibai	Garnet pyroxenite	U–Pb	Zircon	1312 ± 16	Pan et al., 2005
Zhibai	Metapelite	Sm–Nd	Isochron	1770	Burg et al. (1998)
Tongmai	Felsic gneiss	U–Pb	Zircon	564	Zhu et al. (1995)
Daguoqiao	Felsic gneiss	Sm–Nd	Isochron	1453 ± 14	Zhu et al. (1995)
Bononggong	Felsic gneiss	Sm–Nd	Isochron	2178 ± 12	Zhu et al. (1995)
Tongmai	Felsic gneiss	Sm–Nd	Isochron	2296 ± 63	Zhu et al. (1995)
Nanga Parbat	Gneiss	U–Pb	Zircon	1850	Zeitler et al. (1993)
Nanga Parbat	Gneiss			1800–3200	Tahirkheli (1996)

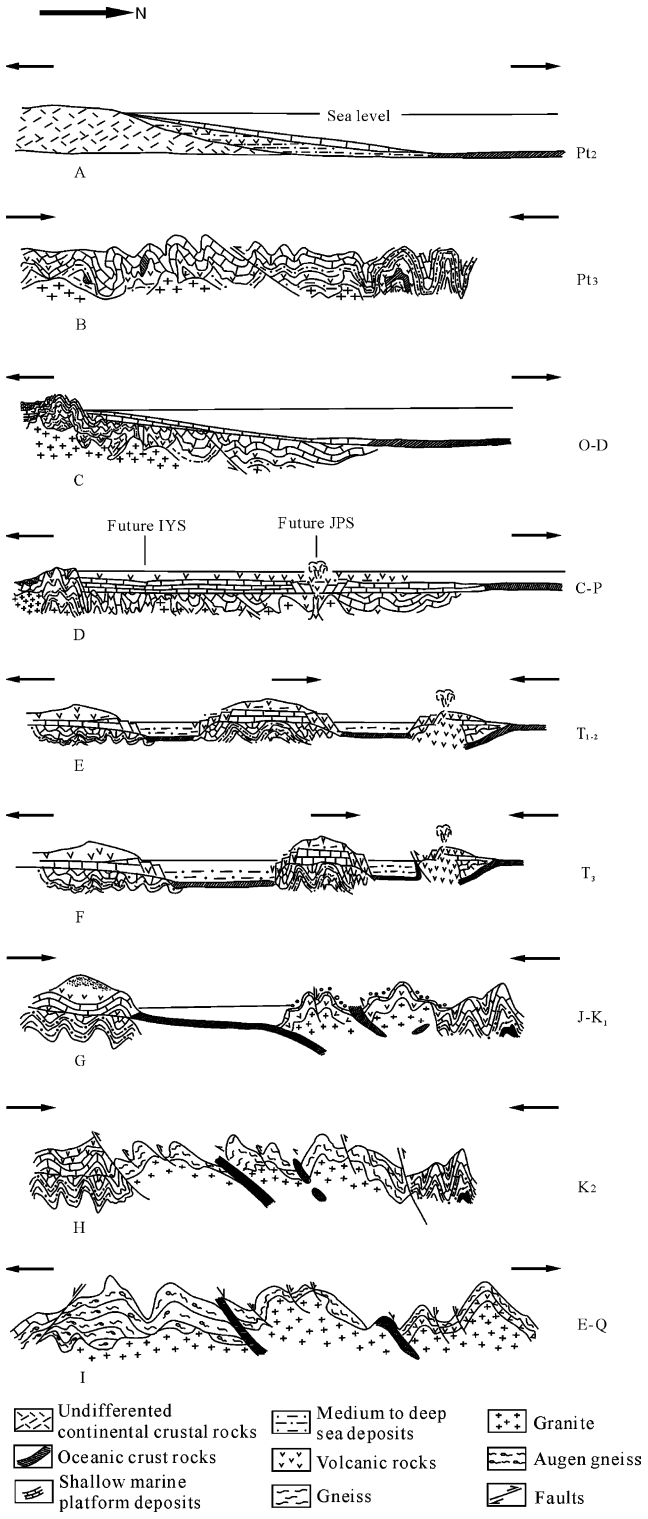

Fig. 8. Proposed regional geologic evolution. Oceanic crust to the north in A, C, D, E and F is considered to be the Bangong-Nujiang Tethys. Some geologists argue that it was the major Tethyan ocean that existed from early Paleozoic until late Mesozoic time (Hsu et al., 1995; Pan et al., 1997). Black arrows for each figure indicate stress directions. (A–B) The northern Indian margin to the south of the Tethyan ocean evolved into a passive carbonate platform in the Late Proterozoic that was then deformed, intruded and eroded to form a land surface of low relief at the end of the Proterozoic. (C–D) The northern Indian passive margin began to break up, rift and subside in the Early Carboniferous. (E–H) Evolution of the Mesozoic Neo-Tethyan archipelago system. The southward subduction of the Neo-Tethyan oceanic crust resulted in the opening and closing of the back arc basins (future IYS and JPS). (I) Cenozoic geology was dominated by crustal folding, strike-slip faulting, denudation and partial crustal melting in the Namche Barwa region. See detailed discussion in the text.

6.3. Mesozoic granites and ophiolite: implications of the collapse of the Neo-Tethys archipelago

During Mesozoic time this region was characterized by three crustal fragments of Precambrian crystalline basement rocks intruded by arc-related plutons and separated by two oceanic belts that are now represented by ophiolitic mélange (Fig. 7 E and F) (Fig. 8E–H). This assemblage indicates that Mesozoic Neo-Tethys was an archipelago system, a tectonic model proposed by Hsu et al. (1995) and Pan et al. (1997). One sample of unmetamorphosed clinopyroxene from an ultramafic fragment at Pangxin yielded an $^{40}Ar/^{39}Ar$ fusion age of 200 ± 4 Ma (Geng et al., 2004), which may imply a crystallization age for the IYS ophiolite. Although we have not obtained a reliable isotopic age for the JPS ophiolite, Middle Jurassic red beds of the Mali Formation unconformably overlie the late Paleozoic rocks along the JPS zone and suggest that the Neo-Tethyan JPS ocean closed at an earlier time than the Neo-Tethyan IYS oceanic realm further south.

Jurassic and Cretaceous granites occur on both sides of the JPS zone and south of the Bangong-Nujiang (BNS) suture (Liu, 1986; Xia and Liu, 1997), which suggest that their origin is related to subduction within the BNS and JPS oceans (Fig. 8 F and G). Subduction began in the IYS Neo-Tethyan ocean in the late Cretaceous as indicated by arc-type granites in the Gangdese magmatic belt with ages that range from 94 to 79 Ma (Table 1). Geochronologic data from high-pressure granulite in the Namche Barwa Group suggest that the India-Asia collision may have occurred between 65 and 70 Ma (Ding and Zhong, 1999; Ding et al., 2001) in this eastern part of the Himalaya. The Neo-Tethyan IYS ocean may have existed only from the Triassic to the end of the Cretaceous and northward subduction within that ocean lasted for only a short period of time in the Late Cretaceous. Geochronological and petrochemical studies show that the Neo-Tethyan oceans, IYS and JPS, were small ocean basins with narrow island arcs between them, supporting the archipelago hypothesis.

6.4. Cenozoic geology: crustal folding, strike-slip faulting, denudation and partial crustal melting

Burg et al. (1997, 1998) and Ding and Zhong (1999) and Ding et al. (2001) documented the Cenozoic geology of the Namche Barwa region and proposed models for uplift (Fig. 8I). Burg and Podladchikov (2002) suggested that uplift and

exhumation of deep seated rocks in the Namche Barwa region was caused by lithospheric folding and erosion, a mechanism they preferred over uniform thickening in a stratified ltihosphere.

Both boundary fault zones on the northwest and southeast sides of the Namche Barwa massif formed to accommodate the northward indentation of the folded Indian plate. The two faults probably link together at the northern end of the Namche Barwa antiform where the Jali fault is present. $^{40}Ar/^{39}Ar$ dating of the metamorphic minerals in the western Dongjiu-Milin fault zone yielded two groups of data related to two series of structures (Zhang et al., 2004). Metamorphic cooling ages following the earlier ductile contractional and lateral-slip deformations yield dates of 62–59 Ma, ~23 Ma and ~13 Ma. The later episode of superposed ductile-brittle normal faulting that dips away from the Namche Barwa antiform occur between 7.3–6.3 Ma.

The Namche Barwa syntaxis was dominated by rapid cooling and denudation since 8 Ma (Ding et al., 2001) and may have developed conditions for partial melting of the crust since 3.9–3.3 Ma due to tectonic decompression as evidenced by leucosome injections (Burg et al., 1998). Fission track dating on the Kohistan granitic batholith in the western syntaxis suggest the exhumation of rocks from ~10 km depth within the last 10 Myr (Zeitler, 1985). In the eastern syntaxis however, isotopic and fission track dating establish cooling and exhumation of rocks from ~30 km depth within the last 4 Myr (Burg et al., 1997).

7. Summary

Detailed field geologic mapping confirmed the previous divisions of tectonostratigraphic domains in the Namche Barwa region by Zhang et al. (1992) and Zhu et al. (1995). The most important achievements made during our geologic projects and field mapping are as follows:

(1) The Precambrian crystalline rocks of the Namche Barwa and Nyainqentanglha Groups are part of the northern Indian plate which stabilized at the end of the Proterozoic. Middle Paleozoic rocks on the northern part of the Indian plate indicate that significant rifting and subsidence began in the early Carboniferous.
(2) Within the Namche Barwa antiform, the Zhibai complex in the lower part of the exposed Indian plate is mainly composed of highly deformed aluminous felsic gneiss containing sporadic boudins of high-pressure granulite. These high-pressure granulite boudins crop out along a northeast trending zone on the northern slope of Himalaya (Fig. 1). The upper part of the Indian plate, the Paixiang Formation, is characterized by an assemblage of layered marble and diopside-bearing calcsilicate rocks within felsic gneiss. The Duoxiongla migmatite crops out in the centeral part of the Namche Barwa massif and could have been generated by anatexis during depressional exhumation ~4 Ma ago.
(3) The eastern continuation of the IYS suture in the Namche Barwa area forms a continuous belt of mélange and includes sporadic ultramafic and mafic lenses from a dismembered ophiolite suite. Geochemical studies suggested that the IYS mélange contains oceanic rocks from the fore-arc, island arc and back-arc basin environments, which implies a SSZ-type (supra-subduction zone) ophiolite setting (Pearce et al., 1984).
(4) The Jiali-Parlung Tsangpo remnant ophiolite-bearing mélange belt may represent a branch of the Neo-Tethyan ocean in Mesozoic time that closed in the early Jurassic. Closure of the oceanic region is demonstrated by unconformable overlapping of Middle Jurassic continental sediments of the Mali Formation. Mesozoic granitic plutons in the northern part of the Gangdise arc are related to subduction within the Bangong-Nujinag and the Jiali-Parlung Tsangpo Neo-Tethyan oceans and was followed by tectonic collision between India and Asia during mid-Cretaceous time. The earliest granitic intrusive rocks derived from subduction within the the IYS Neo-Tethys are late Cretaceous (94 to 79 Ma), while the Cenozoic granitic rocks (17–18 Ma) are the result of melting due to crustal thickening and collapse during Himalayan post-collisional orogenesis.

The northwest and southeast boundary fault zones of the Namche Barwa antiform are characterized by early strike-slip faulting and later ductile–brittle normal faulting. Rapid uplift and exhumation occurred ~4 Ma ago and may be the dominant tectonic processes today.

Acknowledgements

A project 2002CB412609 in the '973' program 'mineralization along the India-Asia collisional zone' helped our publication of this paper. This work is based on the report of 'Regional Geologic Mapping Project in Medog Area of Tibet, scale 1:250,000', which was funded by CGS (Project No. H46C003004). More than 20 geologists were involved in this project, which undertook the most difficult work during two summers in a geologically complicated area. The final manuscript benefited from reviews by Professors B.C. Burchfiel, A. Yin and K. Burke. Professor Burchfiel kindly corrected and rewrote the manuscript to improve its quality. We would like to thank Professors Peter Zeitler, Anne Meltzer at Leigh University USA, Professor Bill Kidd at the University at Albany NY, USA and Professor J.-P. Burg for their helpful discussion and references. We also thank Ms. Kate Bauer for her help with our English writing.

Appendix. Geochemical and geochronological data

Table A1
Petrochemical analyses for metamorphic basalts and ultramafic rocks in the IYS mélange (wt%)

	1	2	3	4	5	6	7	8	9	10	11	12	13	14	15	16	17	18	19	20	21
SiO_2	55.4	52.7	54.1	54.74	53.62	45.8	53.96	45.5	48	49	50.5	55.12	46.42	47.7	50.44	55.02	48.12	45.1	46.2	49.38	55.9
Al_2O_3	12.62	13.17	14.23	14.18	17.1	13.05	13.7	14.8	14.97	14.4	16.68	14.95	15.41	18.51	15.69	14.26	13.2	15.77	12.5	13.2	4.24
TiO_2	2.21	2.85	1.82	2.9	0.84	4.41	1.76	4	1.45	1.28	0.75	1.69	2.23	0.85	1.08	1.88	0.64	0.23	0.53	0.64	0.28
Fe_2O_3	2.73	1.89	2.43	3.33	3.83	4.05	3.94	1.74	1.12	2.55	3.98	4.86	4.54	4.29	2.09	4.09	5.57	5.01	5.88	2.66	1.11
FeO	8.14	9.91	5.65	5.75	4.46	12.88	6.49	13.25	9.05	9.4	6.13	6.01	8.02	6.31	6.06	5.05	4.93	6.74	1.62	3.74	1.32
CaO	8.37	8.44	8.97	6.11	7.64	7.7	9.74	7.12	10.66	9.75	9.36	5.49	4.65	10.38	10.53	6.98	11.08	10.93	23.27	6.03	14.78
MgO	4.58	4.76	5.18	5.21	5.85	5.05	5.17	5.3	7.35	6.41	5.98	4.8	7	5.23	8.99	5.33	10.16	9.92	7.77	6.47	13.43
K_2O	0.58	0.97	0.93	1.84	1.11	1.7	1.31	1.62	0.88	2.09	0.67	3.17	7.42	0.6	0.24	1.15	1.01	0.47	0.045	6.72	0.1
Na_2O	2.38	2.83	3.47	3.43	4.22	2.55	1.55	3.29	2.68	1.71	3.52	1.59	0.27	2.72	2.77	4.09	2.47	1.26	0.37	0.1	1.14
MnO	0.17	0.17	0.14	0.1	0.14	0.28	0.16	0.22	0.19	0.24	0.24	0.19	0.15	0.2	0.14	0.13	0.2	0.17	0.24	0.052	0.08
P_2O_5	0.19	0.3	0.44	0.537	0.248	0.879	0.215	0.6	0.21	0.15	0.237	0.316	0.226	0.06	0.12	0.27	0.24	0.046	0.052	0.12	0.02
LOI	1.21	1.2	0.72	0.48	1.35	1.87	1.8	1.57	2.11	1.96	1.24	2.05	3.17	1.8	0.29	1.66	1.59	3.95	1.14	10.04	5.85
Total	98.58	99.19	98.08	98.61	100.4	100.2	99.8	99.01	98.67	98.94	99.29	100.2	99.51	98.65	98.44	99.91	99.21	99.6	99.62	99.15	98.25

No.	22	23	24	25	26	27	28	29	30	31	32	33	34	35	36	37	38	39	40	41	42
SiO_2	53.8	54.78	53.56	57.32	56.86	48.48	55.48	45.8	46.9	56.06	49.58	44.12	37.52	52.08	55.74	44.78	53.56	57.32	47.3	56.86	41.7
Al_2O_3	6.24	11.92	3.67	2.88	4.13	14.05	13.21	14.85	11.85	15.26	10.92	10.11	13.85	2.3	0.49	8.74	3.67	2.88	0.3	4.13	0.76
TiO_2	0.22	0.36	0.15	0.067	0.13	1.965	2.07	2	0.74	1.58	0.44	0.061	1.14	0.06	0.12	0.067	0.15	0.067	0.018	0.13	0.01
Fe_2O_3	2.17	3.39	4.09	0.81	2.15	4.88	5.68	5.87	5.58	4.95	3.94	1.85	5.15	1.6	5.3	3.71	4.09	0.81	2.02	2.15	1.48
FeO	5.24	7.5	8.8	7.5	6.07	8.61	5.66	7.71	3.7	6.06	5.39	3.54	9.67	4.7	3.47	5.33	8.8	7.5	5.61	6.07	3.6
CaO	10.62	7.58	3.6	5.93	11.11	9.6	7.11	8.12	20.3	7.29	11.38	9.4	7.28	0.01	7.46	1.48	3.6	5.93	0.39	11.11	0.18
MgO	17.31	9.98	20.85	21.66	15.93	4.89	5.41	7.32	6.83	5.38	13.63	24.87	17.96	34.66	23.35	28.16	20.85	21.66	41.2	15.93	49.15
K_2O	0.19	0.41	0.2	0.06	0.1	0.86	0.82	2.63	0.097	0.49	0.42	0.12	0.18	0.1	0.065	0.064	0.2	0.06	0.05	0.1	0.02
Na_2O	0.97	1.55	0.9	0.31	0.7	3.29	1.22	1.62	1.24	0.27	1.36	0.32	0.99	0.26	0.14	0.11	0.9	0.31	0.16	0.7	0.03
MnO	0.24	0.25	0.27	0.26	0.28	0.22	0.18	0.22	0.2	0.16	0.23	0.15	0.19	0.085	0.14	0.062	0.27	0.26	0.091	0.28	0.07
P_2O_5	0.11	0.032	0.038	0.006	0.35	0.326	0.275	0.402	0.24	0.24	0.68	0.011	0.11	0.1	0.016	0.014	0.038	0.006	0.033	0.35	0.09
LOI	0.98	2.15	3.4	2.79	1.1	1.9	3.13	2.72	1.91	1.49	1.64	4.53	5.44	3.88	2.79	7.33	3.4	2.79	2.02	1.1	1.9
Total	98.09	99.9	99.53	99.59	98.91	99.07	100.3	99.26	99.59	99.23	99.61	99.08	99.48	99.84	99.08	99.85	99.53	99.59	99.19	98.91	98.99

Samples 1–31 are metamorphic basalts in the IYS zone: 1–8 between Parlung and Zhaqu, 9–13 between Lugu and Gandai, 14–17 between Pangxin and Yigongbai, 18–20 between Yigongbai and Maniweng, 21–26 between Pangxin and Jiaresa, 27–31 between Yanggudajue and Baila village. Samples 32–42 are ultramafic blocks in the IYS zone: 32,33 in Yanggudajue, 34–37 in Demula, 38 and 40 in Lengduo-Pangxin, 39 in Zongrong, 41 and 42 in Pangxin. All samples have been analysed by atomic absorption spectroscopy for the major elements in Chengdu institute of geology and mineral resources.

Table A2
REE analyses for metamorphic basalts and ultramafic rocks in the IYS mélange (10^{-6})

No.	1	2	3	4	5	6	7	8	9	10	11	12	13	14	15	16	17	18	19	20	21
La	13.98	20.36	15.79	20.49	7.81	42.27	9.93	43.8	5.16	11.78	11.4	21.79	8.6	9.24	2.98	17.2	18.2	0.43	4.42	37.5	11.53
Ce	26.58	39.45	30.52	47.77	18.17	96.61	22.89	87.17	11.06	22.97	26.17	45.83	19.9	16.32	9.36	40.3	35	0.89	11.2	73	21.72
Pr	3.5	4.6	3.45	6.95	2.73	12.96	2.96	9.69	1.4	2.25	3.73	5.91	3.03	1.97	1.99	5.94	4.14	0.12	2.14	11.1	2.13
Nd	17.63	21.93	16.5	31.82	12.81	56.87	13.63	42.66	8.53	10.86	14.99	24.05	14.88	9	7.92	23.3	18.1	0.61	7.79	31.8	8.77
Sm	5.57	6.91	4.88	7.96	3.32	13.15	3.93	11.4	2.94	3.18	3.49	5.46	4.42	2.83	2.81	6.42	4.05	0.24	2.2	6.45	1.98
Eu	1.91	2.43	1.72	3.02	1.05	3.93	1.58	3.28	1.19	1.34	1.066	1.594	1.86	1.43	1.09	2.11	1.11	0.17	0.72	1.05	0.42
Gd	6.39	8.17	5.33	7.73	3.46	13.88	4.95	10.84	4.09	4.73	3.29	5.32	5.34	3.41	3.87	6.7	3.31	0.31	2.47	5.19	1.79
Tb	0.92	1.19	0.73	1.1	0.54	2.11	0.8	1.54	0.55	0.82	0.58	0.922	0.88	0.62	0.69	1.1	0.46	0.05	0.42	0.89	<0.3
Dy	5.75	6.99	4.57	5.22	3.15	12.43	4.74	9.02	4.48	5.63	3.41	5.63	4.91	3.99	4.4	5.71	2.56	0.36	2.39	4.2	1.46
Ho	1.26	1.31	0.79	0.9	0.64	2.31	0.98	1.74	1.11	1.17	0.67	1.1	0.93	0.78	1.01	1.2	0.55	0.08	0.53	0.98	0.29
Er	3.21	3.25	2.01	2.22	1.95	6.69	2.66	4.32	2.97	3.33	2.09	3.5	2.59	2.14	2.64	2.83	1.52	0.24	1.4	2.31	0.78
Tm	0.43	0.45	0.27	0.29	0.3	1	0.41	0.62	0.44	0.49	0.316	0.549	0.36	0.34	0.4	0.43	0.21	0.04	0.19	0.4	0.11
Yb	2.48	2.86	1.72	1.51	1.84	5.95	2.64	3.89	2.52	3.3	1.95	3.67	2.06	2.03	2.53	2.41	1.41	0.23	1.18	2.25	0.74
Lu	0.4	0.42	0.26	0.2	0.27	0.88	0.43	0.64	0.4	0.46	0.276	0.534	0.27	0.32	0.38	0.36	0.21	0.05	0.19	0.37	<0.1
Y	30.03	35.97	21.73	23.91	17.87	62.1	24.82	47.23	26.13	32.99	18.25	31.66	25.37	20.6	22.1	25.9	12.9	1.68	11.7	18.8	8.04

No.	22	23	24	25	26	27	28	29	30	31	32	33	34	35	36	37	38	39	40	41	42
La	0.56	1.27	0.57	1.23	2.14	14.17	10.33	11.03	8.09	8.7	75.2	0.7	0.95	0.66	0.85	1.5	0.57	1.23	0.39	2.14	1.09
Ce	1.77	4.54	1.57	3.94	3.09	34.47	23.24	26.4	19.6	20.07	151	2.51	2.89	1.66	2.94	3.8	1.57	3.94	0.88	3.09	1.98
Pr	0.3	0.72	0.21	0.65	0.37	4.703	3.39	3.79	3.87	3.02	19.5	0.58	0.72	0.15	0.65	0.54	0.21	0.65	0.1	0.37	0.17
Nd	1.65	4.72	0.93	1.88	1.42	19.83	15.81	17.86	13.1	13.73	70.6	2.02	2.83	0.66	3.41	1.92	0.93	1.88	0.42	1.42	0.49
Sm	0.67	1.63	0.35	0.44	0.34	4.818	5.07	4.65	3.4	4.55	14.2	0.62	1.25	0.17	1.37	0.45	0.35	0.44	0.15	0.34	0.08
Eu	0.37	0.55	0.11	0.47	0.14	1.533	1.874	1.744	1.01	1.748	3.1	0.26	0.26	0.03	0.29	0.18	0.11	0.47	0.04	0.14	0.013
Gd	0.82	2.01	0.52	0.36	0.37	5.228	5.82	4.58	3.37	5.19	11	0.68	2.26	0.22	1.94	0.48	0.52	0.36	0.19	0.37	0.09
Tb	0.13	0.32	0.08	0.06	0.06	0.871	0.978	0.784	0.59	0.902	1.41	0.11	0.47	0.04	0.33	0.06	0.08	0.06	0.02	0.06	0.012
Dy	0.72	2.02	0.47	0.26	0.33	5.374	5.79	4.4	2.75	5.03	6.12	0.65	3.64	0.17	2.55	0.26	0.47	0.26	0.08	0.33	0.034
Ho	0.15	0.47	0.12	0.06	0.07	1.14	1.05	0.85	0.63	0.95	1.2	0.18	0.89	0.06	0.59	0.07	0.12	0.06	0.02	0.07	0.008
Er	0.38	1.2	0.36	0.19	0.19	3.252	3.08	2.61	1.57	2.75	2.44	0.45	2.76	0.16	1.71	0.15	0.36	0.19	0.06	0.19	0.021
Tm	0.065	0.18	0.08	0.03	0.03	0.469	0.423	0.387	0.23	0.36	0.34	0.08	0.4	0.04	0.25	0.03	0.08	0.03	0.02	0.03	0.003
Yb	0.46	1.2	0.36	0.19	0.24	3.046	2.59	2.41	1.4	2.14	1.87	0.44	2.69	0.2	1.52	0.13	0.36	0.19	0.05	0.24	0.021
Lu	0.066	0.2	0.1	0.03	0.05	0.456	0.35	0.351	0.21	0.282	0.3	0.09	0.4	0.05	0.2	0.03	0.1	0.03	0.02	0.05	0.003
Y	7.16	10.4	2.32	1.07	2.26	29.58	28.32	22.9	12.8	25.22	23.1	3.53	20.4	1	14	1.32	2.32	1.07	0.19	2.26	0.49

Sample locations see Table A1 in appendix. All samples have been analysed by instrumental neutron activation analysis for the REE at the National Research Center for Geoanalysis, China academy of geosciences, Beijing.

Table A3
Trace elements analyses for metamorphic basalts and ultramafic rocks in the IYS mélange (10^{-6})

No.	1	2	3	4	5	6	7	8	9	10	11	12	13	14	15	16	17	18	19	20	21
V	263	306	198	166	190	408	189	256	284	288	187	189	287	368	173	140	218	241	139	71	26
Cr	87	58	147	107	144	27.2	127	55	180	33	79.1	88.6	159	<5	401	67	309	80	174	64	12
Rb	10	19	18	24.4	16.1	48	36.2	45	15	57	26.2	198	248	9	8.2	16	16	9.1	0.59	62	<2
Sr	275	312	371	512	563	195	358	290	117	97	309	191	328	470	134	379	538	153	884	103	73
Zr	144	167	114	280	507	127	89.5	245	66	57	52	153	111	14	61	113	51	2.3	37	151	92
Nb	8	14	10	21.3	2.7	16.6	7.6	13	<2	<2	2.4	15.5	9	<2	1.8	24	3.3	0.24	2.6	14	4
Ba	149	240	228	373	223	561	112	420	164	158	256	434	448	178	318	411	557	66	101	660	30
Hf	0.4	0.5	0.3	7.2	12.6	3.5	2.7	0.7	0.4	0.7	2.1	4.3	3.3	0.3	1.6	1.7	1.6	0.33	2.1	5.5	<0.2
Ta	0.6	1.1	0.7	2	0.5	1.2	0.78	1.1	0.3	0.3	0.5	1.8	0.86	<0.2	0.45	2	0.51	0.48	0.35	2.5	0.4
Th	6	7	9	2.3	4.8	1.3	1.4	14	8	6	1.3	6.2	1.5	9	0.27	2.8	5.82	0.1	1.1	25	8
Co	26	29	24	28	27	42	22	33	33	32	24	37	44	26	1	14	23	13			5
Ni	29	25	33	72	52	38	31	98	133	56	35	67	35	16	56	42	49	28			10

No.	22	23	24	25	26	27	28	29	30	31	32	33	34	35	36	37	38	39	40	41	42
V	87	166	123	59	144	298	211	229	164	206	171	41	148	38	74	47	123	59	28	144	7.1
Cr	1399	872	1879	2095	1250	79.4	78.1	139	272	75.3	713	1585	1249	1673	2512	494	1879	2095	212	1250	785
Rb	3	11	6.6	5.5	4.6	14.5	15.4	90.3	0.92	4.1	214	0.34	0.66	0.86	0.83	1.6	6.6	5.5	0.36	4.6	<2
Sr	21	24	15	6.6	31	233	199	273	704	209	92	27	43	1.7	23	8.9	15	6.6	2.7	31	4
Zr	<2	31	4.4	3.7	1	138	111	121	56	92.3	52	2.3	73	2	4.1	5.5	4.4	3.7	1.5	1	<2
Nb	<2	1.1	0.43	0.19	0.6	8.5	8.9	5.9	3	8.9	16	0.15	4.1	0.41	0.47	0.81	0.43	0.19	0.3	0.6	<2
Ba	55	59	118	24	16	149	91.9	1373	139	111	779	4.4	286	10	7.6	6.6	118	24	11	16	<30
Hf	<0.2	4.4	1.2	0.64	0.2	5	3.1	3.2	1.9	2.9	1.5	0.73	1.4	0.6	1.7	1.9	1.2	0.64	1.1	0.2	<0.2
Ta	<0.2	0.51	0.41	0.2	<0.2	<0.5	0.95	<0.5	0.7	0.67	0.7	0.48	0.7	0.54	0.2	0.51	0.41	0.2	0.51	<0.2	<0.2
Th	10	0.45	0.13	0.18	0.4	3.6	1.7	<1	1.6	1	22	0.14	0.49	0.31	0.45	0.56	0.13	0.18	0.19	0.4	<5
Co	38	18	19	12	47		29	34.7		27.5			64	69	15	36	19	12	104	47	94
Ni	1045	102	83	204	597		36	81		30			740	1290	352	758	83	204	2890	597	3206

Sample locations see Table A1 in appendix. Trace elements were obtained by inductively-coupled plasma emission spectrometry at the National Research Center for Geoanalysis, China academy of geosciences, Beijing.

Table A4
summary of $^{40}Ar/^{39}Ar$ results

T(C)	^{39}Ar/%	$^{40}Ar/^{*}$%	$^{39}Ar/^{36}Ar$	$^{40}Ar/^{36}Ar$	$^{37}Ar/^{39}Ar$	Age(Ma)	Error
MIVJ-12 biotite (J=0.00099; weight=0.25 g), plateau age=13.7±0.3,isochron age=14.0±0.3							
440	0.66	12.44	82.53	337.55	0.43	9.08	5.45
520	3.99	52.83	482.30	630.27	0.08	12.35	0.68
600	15.09	78.71	1457.68	1426.27	0.02	13.08	0.21
680	29.65	92.59	5117.44	4444.23	0.01	14.42	0.08
750	7.93	76.84	1354.03	1308.06	0.05	13.30	0.31
810	8.72	63.30	737.20	814.21	0.04	12.52	0.36
870	16.28	71.59	980.35	1057.69	0.03	13.83	0.16
1030	14.21	74.73	1176.69	1194.16	0.06	13.59	0.20
1340	3.47	55.72	513.40	671.93	0.49	13.04	0.84
MIVJ-13 biotite (J=0.01004; weight=0.173 g), plateau age=13.2±0.3,isochron age=13.6±0.3							
440	2.07	10.95	71.80	331.90	0.16	9.16	1.56
520	2.74	41.62	371.68	508.08	0.15	10.33	1.22
600	15.03	71.15	1040.12	1042.65	0.02	12.97	0.25
680	26.89	88.46	3249.55	2738.28	0.01	13.57	0.10
750	16.54	80.54	1781.11	1571.25	0.03	12.93	0.23
810	14.26	77.13	1393.62	1325.67	0.03	13.34	0.23
870	14.78	73.79	1180.52	1151.32	0.03	13.08	0.22
1030	6.55	63.09	737.82	809.59	0.13	12.58	0.51
1340	1.13	49.13	336.87	583.21	0.61	15.41	2.91
MIVJ-14 biotite (J=0.009820; weight=0.15 g), plateau age=13.9±0.3, isochron age=14.3±0.3							
440	3.33	7.73	58.35	320.29	0.09	7.51	1.15
520	11.18	50.79	405.34	603.46	0.03	13.41	0.38
600	26.30	80.92	1552.89	1596.21	0.01	14.78	0.10
680	16.21	78.71	1454.54	1426.72	0.03	13.73	0.22
750	8.92	62.86	709.26	804.23	0.06	12.66	0.33
810	12.39	62.30	625.82	791.12	0.05	13.98	0.33
870	12.19	59.93	587.34	743.72	0.06	13.47	0.23
1030	8.03	64.22	659.53	834.39	0.09	14.42	0.35
1340	1.44	40.83	210.96	500.44	0.57	17.13	2.60
MIVJ-16 biotite (J=0.01013; weight=0.23 g), plateau age=16.4±0.3,isochron age=17.0±0.3							
440	12.29	26.77	138.25	403.86	0.03	14.28	0.30
520	15.63	64.38	616.21	837.53	0.03	16.01	0.22
600	31.11	84.01	1724.37	1912.27	0.01	17.06	0.18
680	6.25	78.93	1215.46	1435.04	0.06	17.06	0.52
750	8.71	64.32	587.00	835.68	0.06	16.75	0.38
810	11.09	56.86	480.30	689.53	0.04	14.94	0.27
870	11.90	70.74	793.56	1023.68	0.04	16.70	0.22
1030	2.59	56.71	474.77	687.12	0.16	15.02	1.28
1340	0.43	35.55	111.34	458.90	1.42	26.64	8.39
MIVJ-10-11 biotite (J=0.0102; weight=0.2 g),plateau age=17.3±0.5, isochron age=17.1±0.5							
440	1.64	16.10	162.28	352.44	0.24	6.46	3.08
520	16.68	67.92	687.70	931.56	0.02	16.97	0.22
600	21.62	87.51	2359.74	2484.44	0.01	17.02	0.25
680	12.96	85.23	1938.56	2081.37	0.03	16.90	0.28
750	8.37	81.48	1367.69	1638.29	0.03	18.01	0.43

810	13.46	78.51	1159.78	1405.18	0.02	17.55	0.26
870	20.77	85.83	1932.45	2169.21	0.03	17.78	0.14
1030	3.58	62.96	538.18	804.28	0.22	17.34	0.98
1340	0.92	54.09	228.77	645.61	1.21	27.99	4.04
MIVJ-10-5 muscovite ($J=0.009975$; weight = 0.25 g), plateau age = 16.7 ± 0.3,isochron age = 18.1 ± 0.4							
440	0.64	7.85	68.31	320.71	0.72	6.63	9.07
520	0.94	36.79	172.74	468.20	0.64	17.90	4.93
600	4.47	24.64	201.23	392.60	0.13	8.66	1.33
680	18.3	55.20	383.18	662.90	0.03	17.17	0.26
750	20.31	64.49	599.76	839.98	0.03	16.26	0.21
810	12.03	56.74	445.61	687.26	0.05	15.75	0.37
870	22.23	65.68	620.82	869.57	0.02	16.56	0.18
930	17.62	77.09	1040.05	1315.11	0.03	17.56	0.32
1340	3.45	48.03	294.58	570.58	0.22	16.73	1.20
MIVJ-10-5 biotite ($J=0.0101$; weight = 0.3 g) plateau age = 16.8 ± 0.3, isochron age = 17.3 ± 0.4							
440	2.11	9.51	72.85	326.63	0.13	7.73	1.23
520	11.78	63.26	560.53	811.22	0.02	16.61	0.19
600	28.14	87.84	2336.83	2551.73	0.01	17.43	0.07
680	12.40	86.38	2130.03	2266.69	0.02	16.71	0.20
750	5.83	76.05	1113.90	1258.89	0.05	15.62	0.34
810	11.96	79.01	1241.86	1445.13	0.03	16.71	0.21
870	11.66	81.19	1442.15	1615.74	0.03	16.53	0.26
1030	12.33	81.49	1459.90	1642.02	0.03	16.65	0.18
1340	3.79	72.99	867.44	1110.67	0.25	16.97	0.70
D3556T1 plagioclase ($J=0.0109655$; weight = 0.1009 g), plateau age = 75.27 ± 0.46,isochron age = 79.43 ± 1.34							
350	0.94	67.51	179.46	900.86	0.24	66.22	4.89
550	1.54	81.47	353.51	1545.36	0.37	70.13	3.09
750	8.83	83.32	389.33	1769.73	0.09	73.80	0.57
850	17.68	85.75	467.24	2088.53	0.03	74.53	0.35
950	13.47	87.01	510.78	2270.92	0.09	75.43	0.43
1050	27.56	84.01	398.61	1853.86	0.06	75.98	0.26
1150	21.57	84.47	409.67	1910.04	0.05	76.56	0.37
1250	6.48	82.04	350.90	1634.15	0.14	74.54	1.26
1350	2.01	80.45	297.62	1472.27	0.37	78.02	5.48
MIVTW-23 K-feldspar ($J=0.0109655$; weight = 0.1009 g),plateau age = 74.39 ± 0.56,isochron age = 74.24 ± 1.48							
350	0.86	52.10	111.40	616.95	0.05	56.31	4.42
550	8.45	81.97	402.98	1653.33	0.01	65.48	0.47
750	12.23	84.68	421.00	1943.39	0.02	75.92	0.34
850	15.61	83.49	393.35	1801.66	0.03	74.32	0.32
950	19.25	82.20	344.65	1669.63	0.03	77.31	0.25
1050	27.26	83.87	393.77	1843.95	0.03	76.29	0.22
1150	12.31	82.32	360.70	1682.47	0.02	74.60	0.53
1250	3.12	82.59	360.46	1701.51	0.06	75.80	2.16
1350	1.02	79.95	253.13	1476.21	0.06	90.21	8.88
D3585T2 biotite ($J=0.0109655$; weight = 0.1064 g), plateau age = 96.13 ± 0.54, isochron age = 94.32 ± 1.07							
350	1.02	42.46	38.00	513.54	0.04	110.19	2.54
550	8.45	54.22	68.58	646.13	0.01	98.42	0.32
750	11.59	56.12	76.52	674.12	0.01	95.34	0.25

(*continued on next page*)

T(C)	^{39}Ar/%	$^{40}Ar/^{*}$%	$^{39}Ar/^{36}Ar$	$^{40}Ar/^{36}Ar$	$^{37}Ar/^{39}Ar$	Age(Ma)	Error
850	18.94	53.77	69.03	639.65	0.01	96.05	0.18
950	14.57	83.05	301.46	1752.57	0.02	93.27	0.22
1050	24.57	84.80	332.55	1955.97	0.02	96.27	0.17
1150	12.45	82.06	272.32	1656.26	0.01	96.27	0.36
1250	6.87	53.69	67.30	638.57	0.01	98.15	0.68
1350	1.66	50.15	59.53	593.01	0.03	96.31	3.76
MV(00)T-56 hornblende ($J=0.010997$; weight$=0.1471$), plateau age$=575.20\pm5.24$, isochron age$=582.47\pm11.24$							
500	0.98	55.86	11.832	622.29	20.11	524.88	40.36
700	7.56	60.52	15.20	736.12	3.67	508.13	8.10
850	11.13	63.24	15.13	798.57	1.48	565.85	6.79
950	15.70	61.55	13.43	763.27	1.76	589.20	6.16
1050	19.24	61.85	13.88	769.31	1.67	579.21	5.38
1100	27.56	60.18	12.69	739.11	1.13	589.70	5.45
1150	13.88	61.96	14.14	769.13	2.34	571.48	7.65
1250	3.02	62.79	14.32	775.99	5.34	579.68	25.51
1350	1.04	62.25	13.70	757.21	7.98	588.34	82.56

$^{40}Ar/^{39}Ar$ isotope analyses were conducted on MM-1200 rare gas isotope mass spectrometry at Guangzhou Institute of Geochemistry, CAS.

References

Burchfiel, B.C., Chen, Z., Hodges, K.V., Liu, Y., Royden, L., Deng, C., Xu, J., 1992. The South Tibetan detachment system, Himalayan Orogen: extension contemporaneous with and parallel to shortening in a collisional mountain belt. Geologic society of America 269, 1–41. Special Paper.

Burg, J.-P., Podladchikov, Y., 2000. From buckling to asymmetric folding of the continental lithosphere: numerical modelling and application to the Himalayan syntaxes. In: Khan, M.A., Treloar, P.J., Searle, M.P., Jan, M.Q. (Eds.), Tectonics of the Nanga Parbat Syntaxis and the Western Himalaya, 170. Geological Society, special publications, London, pp. 219–236.

Burg, J.-P., Davy, P., Nieverget, P., Oberli, F., Seward, D., Diao, Z., Meier, M., 1997. Exhumation during crustal folding in the Namche-Barwa syntaxis. Terra Nova 9, 53–56.

Burg, J.-P., Nievergelt, P., Oberli, F., Seward, D., Davy, P., Maurin, J.C., Diao, Z., Meier, M., 1998. The Namche Barwa syntaxis: evidence for exhumation relation related to compressional crustal folding. Journal of Asian Earth Sciences 16, 239–252.

Chamberlain, C.P., Zeitler, P.K., Erickson, E., 1991. Constraints on the tectonic evolution of the northwestern Himalaya from geochronologic and petrologic studies of Babusar Pass, Pakistan. The Journal of Geology 99, 829–849.

Chang, C., Zheng, S., 1973. Tectonic features of the Mount Jolmo Lungma region in southern Tibet, China. Scientia Geologica Sinica 1, 1–12.

Dewey, J.F., Shackleton, R.M., Chang, C., Sun, Y., 1985. The tectonic evolution of the Tibet plateau. Report of the 1985 royal society—Academia Sinica geotraverse of the Qinghai-Xizang plateau. Cambridge University press, Cambridge pp. 379–413.

Diao, Z., Min, J., Liu, Q., 1989. Bomi-Chayu granite belts: rock types and tin mineralization (unpublished report). Chengdu institute of geology and mineral resources, 10–88 in Chinese.

Ding, L., Zhong, D., 1999. Metamorphic characteristics and geotectonic implications of the high-pressure granulites from Namjagbarwa, eastern Tibet. Science in China (Series D) 42, 491–505.

Ding, L., Zhong, D., Pan, Y., et al., 1995. Fission-track evidence for Neogene and Quaternary uplift of the eastern Himalayan Syntaxis. Chinese Science Bulletin 40, 1497–1500 in Chinese.

Ding, L., Zhong, D., Yin, A., Kapp, P., Harrison, M., 2001. Cenozoic structural and metamorphic evolution of the eastern Himalayan syntaxis (Namche Barwa). Earth Planetary Science Letters 192, 423–438.

Gansser, A., 1964. The Geology of the Himalayas. Wiley, New York p. 289.

Garzanti, E., Fort, P.L., Sciunnach, D., 1999. First report of lower Permian basalts in south Tibet: tholeiitic magmatism during break-up and incipient opening of Neotethys. Journal of Asian Earth Sciences 17, 533–546.

Geng, Q., Pan, G., Liu, Y., 2000. Preliminary study on ophiolitic Mélange in the area of Yanlung Tsangpo Graand Canyon, Tibet. Sedimentary Geology and Tethyan Geology 20, 28–43 in Chinese with English Abstract.

Geng, Q., Pan, G., Zheng, L., Liu, Y., Sun, Z., Ou, C., Wang, X., 2001. The Gangdise island-arc granite zone along the Yarlung Zangbo grand canyon, Xizang. Sedimentary Geology and Tethyan Geology 21, 16–22 in Chinese with English Abstract.

Geng, Q., Pan, G., Zheng, L., Sun, Z., Ou, C., Dong, H., 2004. Petrological characteristics and original settings of the Yarlung Tsangpo ophiolitic mélange, Namche Barwa, SE Tibet. Chinese Journal of Geology (formerly Scientia Geologica Sinica) 39, 1–19 in Chinese with English Abstract.

Hao, J., Chai, Y., Li, J., 1999. Original tectonic setting of the Tsangpo ophiolite and sedimentary evolution of the Xigaze forearc basin. Chinese Journal of Geology (Scientia Geologica Sinica) 34 (1), 1–9 in Chinese with English Abstract.

Hickey, R.L., Frey, F.A., 1982. Geochemical characteristics of boninite series volcanics: implications for their source. Geochimie Cosmochimie Acta 46, 2099–2115.

Holt, W.E., Ni, J.F., Wallace, T.C., 1991. The active tectonics of the eastern Himalayan syntaxis and surrounding regions. Journal of Geophysical Research 96, 14595–14632.

Hsu, K.J., Pan, G., Sengor, A.M.C., et al., 1995. Tectonic evolution of the Tibetan plateau: a working hypothesis based on the archipelago model of orogenesis. International Geology Review 37, 473–508.

Li, C., Wang, T., Li, H., Zeng, Q., 2003. Discovery of Indosinian megaporphyritic granodiorite in the Gangdise area: evidence for the existence of Paleo-Gangdise. Geologic Bulletin of China 22 (5), 364–366.

Liu, Z. (Ed.), 1986. Geologic Map of the Tibetan Plateau, 1:1500,000 scale. Geology Publication House, Beijing.

Liu, Y., Zhong, D., 1997. Petrology of high-pressure Granulite from the Eastern Himalaya. Journal of Metamorphic Geology 15, 451–466.

Liu, Y., Zhong, D., 1998. Petrology of high-pressure Granulite from Eastern Himalaya: implications to tectonic significance. Scientia Geologica Sinica 33, 267–281 in Chinese with English Abstract.

Liu, Y., Pan, G., Geng, Q., 2000. The indentation and geologic impacts of the Namche Barwa syntaxis. Sedimentary Geology and Tethyan Geology 20, 52–59 in Chinese with English Abstract.

Pan, G., Chen, Z., Li, X., Yan, Y., Xu, X., Xu, Q., Jiang, X., 1997. Geological–Tectonic Evolution in Eastern Tethys. Geological Publishing House pp. 56–60 (in Chinese with English Abstract).

Pan, G., Liu, Y., Zheng, L., Geng, Q., Wang, L., Li, G., Yin, F., Liao, Z., Zhu, D., 2005. Qinghai-Tibet plateau: collisional tectonics and their effects. Guangdong Science and Technology 12–153 (in Chinese with English Abstract).

Pearce, J.A., Mei, H., 1985. Volcanic rocks of the Tibet geotraverse: Lhasa to Golmud, In: The Geologic Evolution of Tibet. Report of the 1985 royal society—Academia Sinica geotraverse of the Qinghai-Xizang plateau. Cambridge University press pp. 169–201.

Pearce, J.A., Lippard, S.J., Roberts, S., 1984. Characteristics and significance of supra-subduction zone ophiolite. In: Marginal Basin Geology. Geologic Society, London, Special Publication 16, pp. 77–94.

Ratschbacher, L., Frich, W., Chen, C., Pan, G., 1995. Cenozoic deformation, rtation, and stress patterns in eastern Tibet and western Sichuan, China. In: Yin, A., Harrison, T.M. (Eds.), The Tectonics of Asia. Cambridge University Press, New York, pp. 227–249.

Searle, M.P., Cooper, D.J.W., Rex, A.J., 1988. Collision tectonics of the Ladakh-Zansker Himalaya. In: Shackleton, R.M., Dewey, J.F., Windley (Eds.), From the Proceedings of a Royal Society Discussion Meeting, Tectonic Evolution of the Himalayas and Tibet. London University Press, Cambridge, pp. 117–150.

Sobolev, A.V., Danyushevsky, L.V., 1994. Petrology and geochemistry of boninites from the north termination of the Tonga Trench: constraints on the generation conditions of primary high-Ca boninite magmas. Journal of Petrology 35, 1183–1211.

Tahirkheli, R.A.K., 1996. Tectonostratigraphic domains of northern collisional belts in Pakistan (map). Geoscience Laboratory, Geological Survey of Pakistan.

Wang, T., 1993. The petrology and metamorphism of the Aniqiao ductile deformation and metamorphic belt in Moto county, Tibet. Tibet geology 1, 77–85 in Chinese with English Abstract.

Wang, Y., Qu, Y., Lu, P., Wang, Z., Zhang, S., 2003. The geologic feature of ophiolite zone in the Yongzhu area, Tibet. Jilin Geology 22 (2), 1–14 in Chinese with English Abstract.

Winslow, D.M., Zeitler, P.K., 1996. Geochronologic constraints on syntaxial development in the Nanga Parbat region, Pakistan. Tectonics 15, 1292–1308.

Xia, D., Liu, S. (Eds.), 1997. Stratigraphy (Lithostratic) of Xizang Autonomous Region. China University of Geosciences Press, pp. 72–83 in Chinese.

Yang, R., Li, C., Chi, X., Wang, T., 2003. The primary study of geochemical characteristics and tectonic setting of ophiolite in Yongzhu-Namuhu, Tibet. Geoscience 17 (1), 15–19 in Chinese with English Abstract.

Yin, A., Harrison, T.M., 2000. Geologic evolution of the Himalayan–Tibet orogen. Annual Review of Earth Planetary Science Letters 28, 211–280.

Zeitler, P.K., 1985. Cooling history of the NW Himalaya, Pakistan. Tectonics 4, 127–151.

Zeitler, P.K., Chamberlain, C.P., Smith, H.A., 1993. Synchronous anatexis, metamorphism, and rapid denudation at Nanga Parbat (Pakistan Himalaya). Geology 21, 347–350.

Zeitler, P.K., Meltzer, A.S., Koons, P.O., Craw, D., Hallet, B., Chamberlain, C.P., Kidd, W.S.F., Park, S.K., Seeber, L., Bishop, M., Shroder, J., 2001. Erosion himalayan geodynamics, the geomorphology of metamorphism. GSA Today 11 (1), 4–9.

Zhang, Q., Zhou, Y., 2001. Ophiolite of China. Press of Science, Beijing pp. 85–92 (in Chinese with English Abstract.

Zhang, Z., Liu, Y., Wang, T., Yang, H., Xu, B., 1992. Geology in the Namche Barwa area. Science Press, 106–185 in Chinese.

Zhang, J., Ji, J., Zhong, D., Ding, D., He, S., 2004. Structural pattern of eastern Himalayan syntaxis in Namjagbarwa and its formation process. Science in China Series D 47 (2), 138–150.

Zheng, X., Chang, C., 1979. Geologic structural features in lower reaches of Yarlung tsangpo. Scientia Geologica Sinica 2, 116–126 in Chinese with English Abstract.

Zheng, L., Dong, H., Geng, Q., Sun, Z., Liao, G., Lou, X., Li, S., Ou, C., Wang, X., 2003a. Geologic report of regional mapping in Medog (unpublished report). Chengdu Institute of Geology and Mineral Resources, 35–150 in Chinese.

Zheng, L., Geng, Q., Dong, H., Ou, C., Wang, X., 2003b. The discovery and significance of the relicts of Ophiolitic Mélanges along the Parlong Zangpo in the Bomi region, eastern Xizang. Sedimentary Geology and Tethyan Geology 23 (1), 27–30 in Chinese with English Abstract.

Zhong, D., Ding, L., 1996a. Discovery of high-pressure basic granulites in Namjagbarwa area, China. Chinese Science Bulletin 41, 87–88.

Zhong, D.L., Ding, L., 1996b. Rising process of Qinghai–Xizang (Tibt) plateau and its mechanism. Science in China, Series D 39, 369–379.

Zhu, W., Dang, Y., Zhang, X., Li, T., Yang, Q., Ou, C., 1995. Geologic report of regional mapping in Tongmai and Bomi (unpublished report). Gansu Geology and Mineral Resources Bureau, 20–80 in Chinese.